Journal of Magnetic Resonance 200 (2009) 267–279

Contents lists available at ScienceDirect

Journal of Magnetic Resonance

journal homepage: www.elsevier.com/locate/jmr

Supercycled symmetry-based double-quantum dipolar recoupling of quadrupolar spins in MAS NMR: I. Theory

Mattias Edén *, Andy Y.H. Lo

Physical Chemistry Division, Arrhenius Laboratory, Stockholm University, SE-106 91 Stockholm, Sweden

ARTICLE INFO

Article history:
Received 14 May 2009
Revised 4 July 2009
Available online 12 July 2009

Keywords:
Double-quantum coherence
Half-integer spin quadrupolar nuclei
Average Hamiltonian theory
AHT
Magic-angle spinning
Symmetry-based pulse sequences
Low-power recoupling

ABSTRACT

Using average Hamiltonian (AH) theory, we analyze recently introduced homonuclear dipolar recoupling pulse sequences for exciting central-transition double-quantum coherences (2QC) between half-integer spin quadrupolar nuclei undergoing magic-angle-spinning. Several previously observed differences among the recoupling schemes concerning their compensation to resonance offsets and radio-frequency (rf) inhomogeneity may qualitatively be rationalized by an AH analysis up to third perturbation order, despite its omission of first-order quadrupolar interactions. General aspects of the engineering of 2Q-recoupling pulse sequences applicable to half-integer spins are discussed, emphasizing the improvements offered from a diversity of supercycles providing enhanced suppression of undesirable AH cross-terms between resonance offsets and rf amplitude errors.

© 2009 Elsevier Inc. All rights reserved.

1. Introduction

Following the successful introduction of techniques for restoring and utilizing homonuclear through-space dipolar interactions among spin-1/2 nuclei under magic-angle-spinning (MAS) conditions [1–3], increasing efforts have in recent years been made for designing analogous dipolar recoupling tools for half-integer spin quadrupolar nuclei [4–21]. To minimize losses of the central-transition (CT) signals, the first generation of homonuclear recoupling techniques avoided application of radio-frequency (rf) pulses and relied on the non-commutation between homonuclear couplings and other anisotropic interactions, such as heteronuclear couplings to ^{1}H or first-order quadrupolar interactions [4–13]. The main obstacle with such approaches is their dependence of the dipolar recoupling on the particular spin system parameters and on the choice of spinning frequency. Consequently, more recent progress in this area has focussed on rf-driven homonuclear recoupling methodology [14–20], as reviewed in Ref. [21].

The present work concerns double-quantum (2Q) recoupling, which generates a two-spin double-quantum (2Q) dipolar Hamiltonian. Such options have been proposed for the purposes of either driving magnetization transfers between the CT of the recoupled half-integer spins [15,16], or for exciting two-spin CT double quantum coherence (2QC) [17–20]. As will be examined further in this article, the latter category of dipolar recoupling schemes may be viewed as supercycles of 2Q-HORROR irradiation [22] and generalizations thereof [23,24], meaning that the rf amplitude matches 1/2 of the MAS frequency. Mali et al. developed this method further and introduced it for half-integer spins [18]. Subsequent 2Q-recoupling options introduced by us [19,20] exploited symmetry-based pulse sequences [3] that provided improved 2QC excitation performance. Particularly, the $R2_2^1R2_2^{-1}$ scheme of Ref. [19] has found several applications, such as for establishing 2Q–1Q correlations [19], estimating internuclear distances [25] and determining quadrupolar tensor orientations [25,26]. Very recent modifications of this pulse sequence have also been exploited for 2Q–1Q correlation spectroscopy in the context of ^{1}H NMR [27] and for half-integer spins under double-rotation (DOR) conditions [28,29].

Several requirements apply for an "ideal" homonuclear dipolar 2Q-recoupling pulse sequence for half-integer quadrupolar spins: (**I**) It should effect a pure CT 2Q Hamiltonian, which delivers as high double-quantum filtering (2QF) efficiency as possible and is (**II**) associated with a minimum spatial orientation-dependence. Failure to meet this criterion leads to reduced double-quantum filtering (2QF) efficiencies from powders due to destructive interferences between the 2QC amplitudes stemming from different crystallites and determinations of geometry- and distance-related spin-system parameters are hampered. Furthermore, the recoupling should be invariant to (**III**) spreads in resonance frequencies among the spin sites, that may originate both from isotropic chemical and second-order quadrupolar shifts; (**IV**) rf amplitude errors and their fluctuations over the sample length ("rf inhomogeneity")

* Corresponding author.
E-mail address: mattias@physc.su.se (M. Edén).

1090-7807/$ - see front matter © 2009 Elsevier Inc. All rights reserved.
doi:10.1016/j.jmr.2009.07.007

and (**V**) the time-dependent first-order quadrupolar interaction. Finally, all this needs to be achieved by (**VI**) using the lowest possible CT nutation frequency ($\omega_{\rm nut}^{\rm CT}$), so as to be CT-selective and minimize signal losses due to the excitation of single-spin multiple-quantum coherences [13,30,31]. Primarily, pulse sequences operating at the rotary resonance conditions $\omega_{\rm nut}^{\rm CT} = n\omega_r$ ($n = 1, 2, \ldots$) must be avoided.

All requirements but (**V**) apply to all dipolar recoupling scenarios, irrespective of the spin number S. However, while low-power rf operation is desirable for recoupling spins-1/2 (particularly in organic solids), it is an absolute must for half-integer spins and has major bearings on the pulse sequence engineering: A low spin nutation frequency naturally leads to a strong resonance offset-dependence of the dipolar recoupling. A more fundamental problem, however, is the presence of first-order quadrupolar interactions for $S > 1/2$: not only do they interfere with the recoupling, but they also constitute a major hurdle for developing theoretical analyses. The most commonly employed pulse-sequence design framework of average Hamiltonian theory (AHT) is generally carried out in an interaction-frame of the strongest NMR interaction [32–37]. As opposed to the case of quadrupolar nuclei, the rf amplitude may for spins-1/2 readily be arranged to dominate the size of all other NMR interactions. In the absence of rf pulses, a first-order quadrupolar interaction-frame have been employed to gain theoretical insight into quadrupolar-driven homonuclear dipolar "self-recoupling" processes [6,7,9,11–13]. However, the additional presence of rf fields complicate such analyses severely and a rigorous theory for the dynamics of dipolar-coupled quadrupolar spins during a simultaneous application of rf pulses and MAS is hitherto lacking.

The present paper seeks to rationalize the reasoning behind the pulse design amounting in the recoupling techniques presented in Refs. [18–20], as well as to compare their relative advantages and limitations from a theoretical AHT standpoint, particularly their (lack of) adherence to the requirements (**I–V**), and the resulting compensation to rf inhomogeneity (**IV**) and dispersions in resonance frequencies (**III**). To this end, an approximate spin-1/2-based AHT formulation is employed, with focus on comparing the increased robustness of the recoupling resulting form the use of "supercycles" to improve the suppression of undesirable higher-order AH terms.

Extrapolating results from spin-1/2-oriented AHT analyses to the case of the CT of half-integer quadrupolar spins should be exercised with caution. Nevertheless, as shown in Refs. [18,19,25,29], spin-1/2-based AHT predictions (that effectively ignore quadrupolar interactions) are *qualitatively* correct in the following two aspects: (i) The symmetry-based recoupling/suppression of either time-independent (e.g., isotropic chemical shifts) or "small" time-dependent NMR interactions (such as homonuclear dipolar couplings) are to first-order AHT representative also for quadrupolar spins. (ii) For a given pulse sequence, the dipolar scaling factor agrees with predictions made from spin-1/2-stemming theories.

This article is organized as follows: The next section introduces the rf pulse sequences under examination and the experimental protocol used for 2QC excitation, whereas Section 3 reviews some notation used for the remaining of the paper. The details of the AHT formalism employed is given in Appendix. Section 4 gives the pulse sequence-design rationale [subject to the constraint (**VI**)] and compares the 2Q-Hamiltonian forms on a common symmetry-based interpretation with respect to criteria (**I**) and (**II**) above. The response of the 2Q-recoupling schemes to variations in resonance offsets and rf errors [criteria (**III**) and (**IV**)] are examined to third-order AHT in Section 5. Section 6 compares the analytical predictions with numerically calculated 2QF efficiencies offered by the various recoupling schemes in the absence of quadrupolar interactions.

In a forthcoming paper, we will present a comprehensive numerical and experimental survey of half-integer spins subject to quadrupolar interactions.

2. Homonuclear double-quantum recoupling sequences

The properties of many symmetry-based CN_n^v and RN_n^v-based pulse schemes are discussed in Refs. [3,37–41]. Fig. 1(a–c) displays explicit pulse-depictions of the recoupling sequences discussed in this work. The nomenclature CN_n^v and RN_n^v implies that an integral number N of cycles (C) or composite π-pulses (R) extends over n rotational periods $\tau_r = 2\pi/\omega_r$, where ω_r is the MAS frequency. Phase-shifted basic C/R elements are concatenated such that the overall phase ϕ_p added to all pulses in the pth C/R element is given by $\phi_p = 2\pi vp/N$ for CN_n^v and $(-1)^p\pi v/N$ for RN_n^v schemes, with the index running between $p = 0, 1, 2, ..N-1$ [3,37]. N must be even for RN_n^v sequences.

The integers N, n and the sum of flip angles $\beta_{\rm tot}$ of the basic element together require that the spin nutation frequency obeys [3]

$$\omega_{\rm nut} = \frac{N\beta_{\rm tot}\omega_r}{2\pi n}. \tag{1}$$

For $S = 1/2$, the spin nutation frequency $\omega_{\rm nut}$ is identical to the rf nutation frequency,

$$\omega_{\rm nut}^{\rm RF} = |\gamma_S|B_1 \tag{2}$$

where B_1 is the transverse magnetic field component and γ_S the spin gyromagnetic ratio. For CT-selective rf irradiation of an half-integer spin S, it should be arranged that the CT nutation frequency ($\omega_{\rm nut}^{\rm CT}$) obeys Eq. (1). In general, $\omega_{\rm nut}^{\rm CT}$ depends on the quadrupolar frequency

$$\omega_{\rm Q} = \frac{\pi C_{\rm Q}}{S(2S-1)} \tag{3}$$

in a complicated manner, except in the following limits [13,30]:

$$\omega_{\rm nut}^{\rm CT} = \omega_{\rm nut}^{\rm RF} \text{ for } \omega_1 \gg \omega_{\rm Q} \text{ (non-selective irradiation)} \tag{4}$$

$$= \left(S + \frac{1}{2}\right)\omega_{\rm nut}^{\rm RF} \text{ for } \omega_1 \ll \omega_{\rm Q} \text{ (CT-selective irradiation)} \tag{5}$$

$C_{\rm Q} = e^2qQ/h$ is the quadrupolar coupling constant.

In this work, R either represents a π_0-pulse or the composite pulse $(\pi/2)_0(3\pi/2)_\pi$, whereas C is a multiple of a 2π pulse. The present symmetry-numbers (N, n and v) implies that all recoupling schemes (i) employs a spin-S CT nutation frequency related to the MAS frequency as $\omega_{\rm nut}^{\rm CT} = \omega_r/2$ and (ii) are "amplitude-modulated", meaning that the phases of two arbitrarily selected pulses are related to each other by $\phi_q = \phi_p + K\pi$ with $K = 0$ or ± 1. It may be verified from Fig. 1 that the present sequences are constructed by concatenating rf pulses with phases $\pi/2$ or $3\pi/2$. The CN_n^v symmetries depicted in Fig. 1c convey different 2Q-HORROR implementations, as explained in Sections 4 and 5.

We primarily consider $CN_n^vCN_n^{-v}$, RN_n^v RN_n^{-v} or $R2_4^1[\overrightarrow{X}, \overleftarrow{X}]$ supercycles. A phase inversion $RN_n^vRN_n^{-v}$ scheme represents a concatenation of two RN_n^v and RN_n^{-v} cycles [3,40,42], whereas $R2_4^1[\overrightarrow{X}, \overleftarrow{X}]$ is based solely on $R2_4^1$ symmetry but employing a flip-angle permutation within the R-elements such that $\overrightarrow{X} = (\pi/2)_0(3\pi/2)_\pi$ and $\overleftarrow{X} = (3\pi/2)_0(\pi/2)_\pi$ [20]. Note that $R4_4^2$ symmetry simply constitutes two repeated $R2_2^1$ cycles and that $R4_4^2R4_4^{-2}$ is identical to a $R2_2^1R2_2^1R2_2^{-1}R2_2^{-1}$ sequence [19]. We consider $R4_4^2R4_4^{-2}$ as it has in practice often turned out (somewhat surprisingly) to give better 2QC excitation than $R2_2^1R2_2^{-1}$ [19,20].

"MQ phase-cycling" represents another supercycling nesting level [35,40,42–46]. Here we only consider the special case of "$M = 2$" cycles, denoted $(RN_n^vRN_n^{-v})2^1$ and corresponding to a concatenation of a phase-inversion supercycle with its counterpart

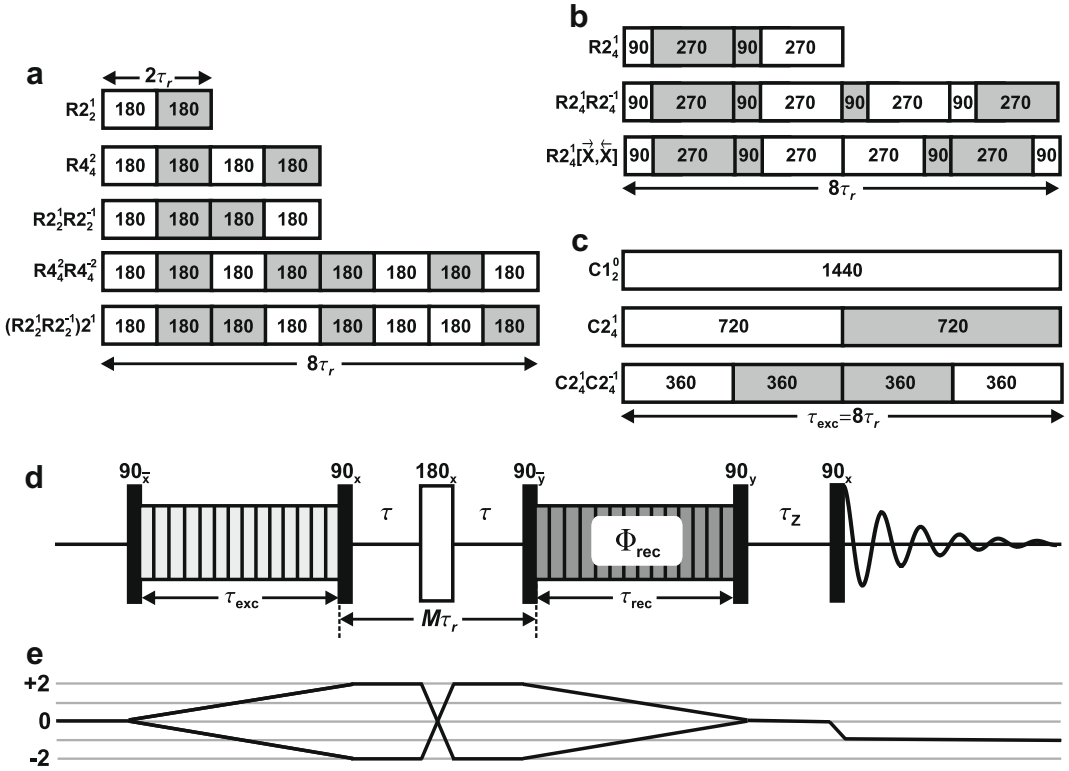

Fig. 1. (a and b) Symmetry-based RN_n^ν pulse sequences constructed from the following inversion elements: (a) R = π_0; (b) R = $\overrightarrow{X} \equiv (\pi/2)_0(3\pi/2)_\pi$ and $\overleftarrow{X} \equiv (3\pi/2)_0(\pi/2)_\pi$. Each pulse is depicted by a box, with the flip angle (in degrees) given by the inset number, and rf phases of $\pi/2$ or $3\pi/2$ represented by white and gray color, respectively. (c) CN_n^ν schemes illustrating implementations of various HORROR versions for the case $\tau_{exc} = 8\tau_r$ and corresponding to $C = (2p\pi)_{\pi/2}$ with $p = 4$ ($C1_8^0$; HORRORy), $p = 2$ ($C2_8^1$; HORRORy$\bar{y}$) and $p = 1$ ($C2_4^1C2_4^{-1}$; HORRORy$\bar{y}\bar{y}$y). See Section 4.1 and Table 2 for further information. All recoupling pulses in (a–c) operate at $\omega_{nut}^{CT} = \omega_r/2$, with ω_{nut}^{CT} given by Eqs. (4) and (5) for non-selective and CT-selective conditions, respectively. Only the $(R2_2^1R2_2^{-1})2^1$ "$M = 2$" supercycle is displayed; all others span $16\tau_r$. (d) Double-quantum filtering (2QF) rf pulse scheme, using the dipolar recoupling sequences in (a)-(c) for 2QC generation and reconversion during the intervals $\tau_{exc} = \tau_{rec}$ [18–20,25,26]. Black rectangles represent $\pi/2$ pulses. Each pulse train is sandwiched between two CT-selective $\pi/2$-pulses of rf phases π (left pulse) and 0 (right pulse) for optimal 2QC excitation. τ_z marks a z-filter interval. (e) Coherence-transfer pathway, indicating the desirable coherence conversions by black lines.

resulting from a shift of all rf-phases by π : $[RN_n^\nu RN_n^{-\nu}]_0[RN_n^\nu RN_n^{-\nu}]_\pi$ [40,42]. The same construction principle applies to $(CN_n^\nu CN_n^{-\nu})2^1$ and $\left(R2_4^1[\overrightarrow{X},\overleftarrow{X}]\right)2^1$ schemes.

Due to the small numbers of N, n and ν used in the RN_n^ν and CN_n^ν hierarchies considered, coupled to the simple basic pulse-elements employed, several equivalent formulations exist within the symmetry-based framework for the schemes shown in Fig. 1. For example, as rf phases of consecutive pulses are related by π, any phase-inversion supercycle of this work, $R2_n^1R2_n^{-1}$ or $C2_n^1C2_n^{-1}$, may be expressed alternatively as $\left(R2_n^1\right)2^1$ and $\left(C2_n^1\right)2^1$, respectively. Further, any $R2_n^1R2_n^{-1}$ scheme built from an amplitude-modulated inversion element R may be expressed as a $C2_{2n}^1$ sequence based on a cyclic element C. The latter is constructed by concatenating R with its π-shifted counterpart (giving RR_π) and next shifting all rf-phases by $\pi/2$. This results in $C \equiv [R_{\pi/2}R_{3\pi/2}]$ and the following pulse sequence equivalence:

$$R2_n^1R2_n^{-1} \Longleftrightarrow C2_{2n}^1 \text{ with } C \equiv (R_{\pi/2}R_{3\pi/2}) \tag{6}$$

For instance, the $R2_2^1R2_2^{-1}$ scheme of this work is identical to a $C2_4^1$ pulse train built on the cyclic element $C = \pi_{\pi/2}\pi_{3\pi/2}$. Similarly, for an amplitude-modulated cyclic element C combined with $C2_n^1$ symmetry, it holds that

$$C2_n^1C2_n^{-1} \Longleftrightarrow C'2_{2n}^1 \text{ with } C' \equiv CC_\pi \tag{7}$$

Several hierarchical relationships between the various dipolar recoupling schemes of this work will be examined in Sections 4 and 5.

Fig. 1d shows the experimental rf pulse scheme for creating 2QC involving solely the central transitions of half-integer quadrupolar spins [18,19]. On sandwiching each dipolar recoupling pulse-train between two CT-selective $\pi/2$-pulses (black rectangles) of duration τ_{90}^{sel} and rf phases π and 0, respectively, dipolar recoupling is active during τ_{exc} for driving each of the $S_z^{CT} \rightarrow 2QC^{CT}$ and $2QC^{CT} \rightarrow S_z^{CT}$ transfers. The phase-shift $\Phi_{rec} = \pi/2$ is applied to all pulses associated with the latter process, including the bracketing $\pi/2$-pulses. S_z^{CT} and $2QC^{CT}$ represent the total longitudinal CT magnetization and CT 2QC operators of the spin-pair, respectively. A coherence transfer diagram is depicted in Fig. 1e and its implementation by phase-cycling is described in the Supporting Information.

3. Theoretical analysis: Overview

3.1. Spin Hamiltonian

Consider a pulse sequence of N_p pulses associated with rf phases $\{\phi_1, \phi_2, \ldots, \phi_{N_p}\}$ and durations $\{\tau_1, \tau_2, \ldots, \tau_{N_p}\}$. The scheme starts at time-point $t = t_0 = 0$ and the pth pulse is active between $t = t_{p-1}$ and $t = t_p$. The total pulse train spans an interval T. We assume that the nominal ("ideal") rf amplitude is constant throughout the sequence [Eq. (2)]. The rotating-frame rf Hamiltonian during the pth pulse may be expressed as follows

$$H_{RF} = \left(\omega_{nut,nom}^{RF} + \omega_\varepsilon\right)R_z(\phi_p)S_xR_z(-\phi_p), \quad t_{p-1} \leqslant t < t_p \tag{8}$$

$$= H_{RF}^{nom} + H_{RF}^{\varepsilon} \tag{9}$$

where

$$\omega_\varepsilon = \omega_{\mathrm{nut}}^{\mathrm{RF}} - \omega_{\mathrm{nut,nom}}^{\mathrm{RF}} \tag{10}$$

represents the deviation of the actual rf nutation frequency from its nominal value. Eq. (9) that separates the nominal and rf error Hamiltonians (proportional to $\omega_{\mathrm{nut,nom}}^{\mathrm{RF}}$ and ω_ε, respectively) is used to analyze the impact of rf amplitude errors ("rf inhomogeneity") on the spin dynamics.

Besides rf amplitude errors, $H_{\mathrm{RF}}^{\varepsilon}(t)$, we only consider the time-dependent through-space dipolar interaction between two spin-S j and k, and their respective time-independent isotropic (chemical) shift terms

$$H(t) = H^{jk}(t) + H_{\mathrm{CS}}^{j} + H_{\mathrm{CS}}^{k} + H_{\mathrm{RF}}^{\varepsilon}(t) + H_{\mathrm{RF}}^{\mathrm{nom}}(t) \tag{11}$$

The dipolar Hamiltonian $H^{jk}(t)$ is proportional to orientation-dependent factors involving the Euler angles [47] $\{\alpha = 0, \beta, \gamma\}$ and to the coupling constant $b^{jk} = -(\mu_0/4\pi)\gamma_S^2\hbar r_{jk}^{-3}$, where r_{jk} is the internuclear distance [48]. The angles $\{\beta, \gamma\}$ relate the dipolar vector to a rotor-fixed axis system. We refer to Ref. [48] for detailed Hamiltonian expressions. The net resonance offset frequencies of spins j and k relative to the spectrometer reference ("carrier") frequency are denoted by $\omega_{\mathrm{iso}}^{j}$ and $\omega_{\mathrm{iso}}^{k}$, respectively. They represent isotropic (chemical) shifts, which may also include contributions from second-order quadrupolar shifts [13]. We ignore J-interactions and anisotropic chemical shifts.

As outlined in the Appendix, all AH terms are evaluated in the interaction-frame of the rf Hamiltonian. As opposed to the more correct notation employed in the Appendix, for brevity we omit the "tilde" symbols on top of the average Hamiltonians. We employ an AH analysis accounting for the dipolar interaction to first order. The resulting expressions presented in the next section are valid for any spin number in the limit of non-selective rf irradiation, meaning that the rf nutation frequency far exceeds the quadrupolar frequency ω_{Q} [Eq. (4)]. This effectively amounts to omitting the first-order quadrupolar interactions; their impact on the spin dynamics will be probed by numerical simulations and experiments in the subsequent paper. Alternatively, in the other extreme limit of very weak rf amplitudes that lead to truly CT-selective irradiation [Eq. (5)], the first-order quadrupolar interaction has no direct influence on the CT 2Q-dynamics [13]. This has been the underlying assumption made in all theoretical studies of half-integer spin-recoupling presented thus far [15–18,29]. Some consequences of this approximation were explored numerically in Ref. [29]. The results verified that the 2Q-dynamics of the CT alone is *qualitatively* mimicking that of using the full form of the rf Hamiltonian in the limit of weak pulses but that the 2QF efficiencies are strongly reduced in the presence of first-order quadrupolar interactions.

3.2. $\pi/2$-Sandwiched recoupling sequences

We assume that the $\pi/2$ bracketing pulses are infinitesimally short ("delta" pulses). The consequences of using finite pulse-lengths are minor, as discussed in the Supporting Information. We denote an arbitrary AH term stemming from a "plain" (i.e., non-bracketed) pulse train $\mathscr{S}$ by $\overline{H}^{(n)}_{(\Lambda_j\times\Lambda_k\times\ldots)}$. The corresponding AH term when the same scheme is preceded by a $(\pi/2)_\phi$ pulse and followed by a $(\pi/2)_{\phi+\pi}$ pulse, is labeled $\overline{H}^{(n)}_{(\Lambda_j\times\Lambda_k\times\ldots)}[\mathscr{S}]$. The AH are related by

$$\overline{H}^{(n)}_{(\Lambda_j\times\Lambda_k\times\ldots)}[\mathscr{S}] = R_\phi(-\pi/2)\overline{H}^{(n)}_{(\Lambda_j\times\Lambda_k\times\ldots)}R_\phi(\pi/2). \tag{12}$$

Hence, given our choice of $\phi = \pi$ (Fig. 1d), $\overline{H}^{(n)}_{(\Lambda_j\times\Lambda_k\times\ldots)}[\mathscr{S}]$ is obtained upon a counterclockwise rotation of $\overline{H}^{(n)}_{(\Lambda_j\times\Lambda_k\times\ldots)}$ by $\pi/2$ around the x-axis of the rotating frame. A trivial but important consequence of Eq. (12) is that *if* a given AH term vanishes for a certain pulse train $\mathscr{S}$, it also vanishes for the corresponding bracketed sequence $[\mathscr{S}]$:

$$\overline{H}^{(n)}_{(\Lambda_j\times\Lambda_k\times\ldots)} = 0 \Rightarrow \overline{H}^{(n)}_{(\Lambda_j\times\Lambda_k\times\ldots)}[\mathscr{S}] = 0. \tag{13}$$

4. Theoretical aspects of double-quantum recoupling

4.1. Average dipolar Hamiltonian

The basic requirement **I** (see Section 1) for a 2Q dipolar recoupling pulse sequence is that its average dipolar Hamiltonian solely comprises operators of the form $S_j^+S_k^+$ and $S_j^-S_k^-$ to first order. So-called "γ-encoded" recoupling sequences achieve optimal adherence to requirement (**II**) by effectively restricting the orientation-dependence to one Euler angle (β), whereas the 2QF signal-amplitudes generated from pulse schemes devoid of this property depend on the pair of angles (β, γ) [22]. These cases are associated with ideal 2QF efficiencies of 73% and 52%, respectively [22]. In the context of half-integer spins, the $\pi/2$-sandwiched HORRORy sequence constitutes the sole 2Q-recoupling option fulfilling both criteria (**I**) and (**II**) [18,22]. Using the notation of Ref. [19], the appended "y" denotes the as-assumed rf-phase (Fig. 1c) and distinguishes it from the "HORROR$y\bar{y}$" version introduced by Mali and co-workers [18], which employs phase-reversal at the midpoint $\tau_{\mathrm{exc}}/2$ of the excitation interval (Fig. 1c).

Continuous-wave HORRORy in the *absence* of bracketing pulses provides recoupling of 2Q $\left(\sim S_j^\pm S_k^\pm\right)$, 1Q $\left(\sim S_j^\pm S_{kz}\right)$ as well as ZQ $\left(\sim S_j^\pm S_k^\mp\right)$ dipolar terms [23,24], reflected by the following first order AH:

$$\overline{H}^{jk}_{\mathrm{HORRORy}} = f(b^{jk},\beta)\left\{\cos\gamma\left[-\sqrt{\frac{3}{2}}T_{20}^{jk} + \frac{1}{2}\left(T_{22}^{jk} + T_{2-2}^{jk}\right)\right] + \sin\gamma\left(T_{2-1}^{jk} - T_{21}^{jk}\right)\right\} \tag{14}$$

The function $f(b^{jk}, \beta)$ depends on the dipolar coupling constant and the dipolar vector orientation relative to the rotor-frame z-axis,

$$f(b^{jk},\beta) = \frac{3}{4\sqrt{2}}b^{jk}\sin 2\beta, \tag{15}$$

and $T_{2\mu}^{jk}$ is the μth component of a second rank irreducible spherical tensor operator (e.g., see [47,48]):

$$T_{20}^{jk} = \frac{1}{\sqrt{6}}\left\{2S_{jz}S_{kz} - \frac{1}{2}\left(S_j^+S_k^- + S_j^-S_k^+\right)\right\} \tag{16}$$

$$T_{2\pm1}^{jk} = -\frac{1}{2}\left(S_j^\pm S_{kz} - S_{jz}S_k^\pm\right) \tag{17}$$

$$T_{2\pm2}^{jk} = \frac{1}{2}S_j^\pm S_k^\pm. \tag{18}$$

On the other hand, when sandwiched between two $\pi/2$-pulses of opposite phases, HORRORy effects a pure γ-encoded 2Q Hamiltonian [18,22,24]:

$$\overline{H}^{jk}_{[\mathrm{HORRORy}]} = f(b^{jk},\beta)\left(T_{22}^{jk}\exp\{-\mathrm{i}\gamma\} + T_{2-2}^{jk}\exp\{\mathrm{i}\gamma\}\right). \tag{19}$$

The subscript $[\mathscr{S}]$ implies a $\pi/2$-bracketed sequence $\mathscr{S}$. Note the high scaling factor $3/(4\sqrt{2}) \approx 0.530$ of the recoupled 2Q dipolar terms [Eq. (15)].

From a sole 2Q-recoupling perspective, Eq. (19) is the ideal form of the dipolar Hamiltonian, fulfilling both criteria (**I**) and (**II**). Unfortunately, the 2Q-HORROR option is extremely sensitive to rf inhomogeneity [22,49]. Mali and co-workers remedied this deficiency by proposing the HORRORy$\bar{y}$ scheme [18]. As introduced, the bracketed 2Q–HORRORy$\bar{y}$ technique does not imply any restriction on the sampling of τ_{exc}. As such, it is associated with a rather ill-defined AH, which is γ-encoded throughout the first half of the recoupling interval but becomes non-γ-encoded during its second part. Moreover, chemical shifts (resonance offsets) are recoupled, unless $\omega_{\mathrm{nut}}\,\tau_{\mathrm{exc}}/2$ equals an integer number of 2π pulses. On the

other hand, if it is arranged that $\tau_{exc} = 4p\tau_r$, the bracketed HORRORy$\bar{y}$ implementation may be identified by a (bracketed) $C2^1_{4p}$ sequence with basic element $C = (2p\pi)_{\pi/2}$. The resulting average dipolar Hamiltonian carries a $\cos\gamma$-dependence according to

$$\overline{H}^{jk}_{[\mathrm{HORRORy\bar{y}}]} = f(b^{jk},\beta)\cos\gamma\left(T^{jk}_{22} + T^{jk}_{2-2}\right). \tag{20}$$

The AH dipolar Hamiltonian of the "plain" HORRORy$\bar{y}$ sequence (i.e., $C2^1_{4p}$) is analogous to Eq. (14), except for the absence of $T^{jk}_{2\pm1}$ operators, which are removed by the phase-reversal:

$$\overline{H}^{jk}_{\mathrm{HORRORy\bar{y}}} = f(b^{jk},\beta)\cos\gamma\left\{-\sqrt{\frac{3}{2}}T^{jk}_{20} + \frac{1}{2}\left(T^{jk}_{22} + T^{jk}_{2-2}\right)\right\}. \tag{21}$$

It is instructive to compare the average dipolar Hamiltonians of the various 2Q-HORROR versions, as they represent the prototype forms to which all RN^{ν}_{n} symmetry-based recoupling options introduced in Refs. [19,20,29] conform to. The π-based mixed ZQ/2Q $R2^1_2$ recoupling sequence [19] is associated with the same average dipolar Hamiltonian as HORRORy$\bar{y}$

$$\overline{H}^{jk}_{\mathrm{R2}} = \overline{H}^{jk}_{\mathrm{HORRORy\bar{y}}}, \tag{22}$$

from which the identity of the average Hamiltonians of their respective *bracketed* versions follows directly [19]:

$$\overline{H}^{jk}_{[\mathrm{R2}]} = \overline{H}^{jk}_{[\mathrm{HORRORy\bar{y}}]}. \tag{23}$$

Moreover, as shifting all phases by π within a pulse train leaves its associated 2Q and ZQ dipolar Hamiltonian terms invariant to first order AHT [40], it follows that the AH of all $RN^{\nu}_{n}RN^{-\nu}_{n}$ and $(RN^{\nu}_{n}RN^{-\nu}_{n})2^1$ supercycles also conforms to Eqs. (22) and (23) for the respective "plain" and bracketed pulse schemes. The same holds for the $R2^1_4[\overrightarrow{X},\overleftarrow{X}]$ supercycle.

It deserves noting that (i) both Hamiltonians of Eqs. (22) and (23) excite 2QC from a spin ensemble state of longitudinal polarization [19], but that (ii) the 2QC buildup (in the absence of other interfering spin interactions) is twice as rapid when sandwiching the recoupling pulses by $\pi/2$-pulses. (iii) As discussed further in Section 5.5, the ZQ dipolar terms $\left(\sim S^{\pm}_{j}S^{\mp}_{k}\right)$ of the non-bracketed schemes interfere with the 2Q-recoupling due to the non-commutation of the 2Q and ZQ operators. (iv) Brinkmann and coworkers have provided a route for obtaining the CT operator contribution of an irreducible tensor [29]: those results may be exploited to project out the CT operator contribution $T^{jk}_{\lambda\mu}[\mathrm{CT}]$ from any operator $T^{\Lambda}_{\lambda\mu}$ given in this paper, by using the mapping $T^{\Lambda}_{\lambda\mu} \rightarrow c^{\Lambda}_{\lambda}(S)T^{\Lambda}_{\lambda\mu}[\mathrm{CT}]$, where $c^{\Lambda}_{\lambda}(S)$ is a proportionality constant depending on the rank λ of the tensor and the spin number S [29]. The primary consequence is an acceleration of the CT 2QC excitation by the factor $c^{\mathrm{DD}}_{2}(S)$ compared to the case of $S = 1/2$ recoupling [18,29]. However, note that all our simulation results discussed below solely involved 2QF processes of the central transitions, which were nevertheless successfully interpreted using the full spin operator forms employed throughout this paper. The expressions presented here will also be relevant for future spin-1/2 applications to be discussed elsewhere.

In summary, all recoupling pulse sequences discussed in this work (Fig. 1) may be classified in terms of the generic AH expressions Eqs. (21) and (20) in their "plain" or "bracketed" versions, respectively. However, the various pulse schemes generally differ in their robustness to resonance offsets and rf amplitude errors, as discussed in Section 5.

4.2. Pulse sequence engineering considerations

2Q-recoupling pulse-sequence construction aiming at meeting all of the criteria (**I**)–(**VI**) in the scope of half-integer quadrupolar nuclei is exceedingly difficult/impossible. We have already pointed out the restrictions set by condition (**VI**) for obeying the requirements of resonance offset compensation and to avoid CT signal losses. In practice, the latter become significant unless $\omega^{\mathrm{CT}}_{\mathrm{nut}} < \omega_r$. To ensure reasonably accurate spin manipulations by the rf pulses, in general requiring MAS frequencies exceeding 10 kHz for multi-site samples (and preferably higher than 20 kHz), the window of usable CT spin nutation frequencies is approximately $\omega_r/2 \leqslant \omega^{\mathrm{CT}}_{\mathrm{nut}} < \omega_r$.

Assume that an array of the CT spin-lock signal-amplitudes is recorded *vs* $\omega^{\mathrm{CT}}_{\mathrm{nut}}$ (e.g., see Refs. [15,18]): *provided* that the spread of spin resonance offsets is not too substantial and the rf carrier frequency is positioned at the midpoint of the NMR spectrum, signal losses are generally minimized for $\omega^{\mathrm{CT}}_{\mathrm{nut}} < \omega_r/2$ and $\omega^{\mathrm{CT}}_{\mathrm{nut}} \approx 3\omega_r/4$. The latter condition usually constitutes the optimal operating power for the bracketing pulses, as it is low enough to allow CT-selective operation for samples with widely ranging quadrupolar coupling constants and yet sufficiently large for accurate spin rotations. In principle, it would be beneficial to operate at $\omega^{\mathrm{CT}}_{\mathrm{nut}} \approx 3\omega_r/4$ also during dipolar recoupling, but we have so far not found any pulse scheme that combines pure 2Q recoupling with a sufficiently large dipolar scaling factor and reasonable compensation to resonance offsets and rf inhomogeneity around this rf condition.

The restriction of using rf amplitudes that give CT nutation frequencies within the range $\omega_r/2 \leqslant \omega^{\mathrm{CT}}_{\mathrm{nut}} < \omega_r$ during recoupling strongly limits the available combinations of symmetry-based parameters N, n and basic C and R elements, as dictated by the expression for the nutation frequency $\omega^{\mathrm{CT}}_{\mathrm{nut}}$ in Eq. (1). All symmetry-based 2Q recoupling options developed thus far for spins-1/2 exhibit combinations of N (high) and n (low) that are incompatible with $\omega^{\mathrm{CT}}_{\mathrm{nut}} < \omega_r$. This is a primary reason why robust and frequently employed 2Q-recoupling symmetries such $C7^1_2$ (C7 [50], CMR7 [51] and POST-C7 [52]), $C5^1_2$ (SPC-5 [53]), $C14^5_4$ (SC14 [54]), $R14^6_2$ [39,44,55], $R26^{11}_4$ [41,56] and many others [3,54,57] cannot be utilized for half-integer quadrupolar spins. The same problem applies to analogous spin-1/2 techniques such as DRAWS [58], MELODRAMA [59] and BABA [60]. The sole recoupling of γ-encoded 2Q dipolar terms $(T_{2\pm2})$ is not incommensurate with low rf-field application [3,57]. For instance, $R = \pi$ combined with the symmetries $R18^5_{10}, R18^7_{14}$ and $R20^9_{18}$ provide ratios $\omega^{\mathrm{CT}}_{\mathrm{nut}}/\omega_r$ of 0.90, 0.64 and 0.56, respectively. However, while isotropic shifts are suppressed to first-order and the dipolar scaling factors are decent (>0.1), the long cycle periods of these sequences leads in practice to unacceptably large high-order AH terms associated with isotropic shifts and other undesirable interactions.

We have evaluated a large number of potential symmetry-numbers and basic elements by AHT and numerical simulations of the 2QC excitation dynamics. Here we only discuss those found that fulfill requirements (**I**) and (**II**) (within the sacrifice of γ-encoding [22]), while simultaneously providing reasonable compensation to resonance offsets and rf amplitude errors (i.e., conditions (**III**) and (**IV**). Note that breaking requirement (**I**) necessarily also compromises condition (**II**) due to the simultaneous presence of a multitude of dipolar operators, that are normally associated with distinct spatial orientational dependencies and thereby lead to reduced 2QF efficiencies.

To our knowledge, there do not exist other options to simultaneously fulfill requirements (**I**) and (**VI**) than using *amplitude-modulated* $\pi/2$ pulse-sandwiched recoupling schemes operating at the HORROR condition $\omega^{\mathrm{CT}}_{\mathrm{nut}} = \omega_r/2$. Hence, there is *no coincidence* that all symmetries considered have low ratios of $N/n = 1$ $\left(R2^1_2, R4^2_4\right)$ and $N/n = 1/2$ $\left(R2^1_4, C2^1_4\right)$ and are combined with basic elements giving summed flip angles of π and 2π, respectively. Yet, γ-encoded recoupling needs to be sacrificed to compensate for rf inhomogeneity.

The combination of sandwiching $\pi/2$-pulses and ZQ/2Q recoupling schemes offering ultra-low-power operation adds another

degree of freedom in the dipolar recoupling engineering, as the bracketing pulses rotates the mixed ZQ/2Q operators into a pure 2Q Hamiltonian [Eq. (12)]. We wish to highlight this (old) concept, which after its introduction [22–24] does not appear to have been developed much further, except in Ref. [49] and in the realm of half-integer spins [18–21]. Demonstrations of improved HOR-ROR-type supercycles will be given elsewhere in the context of spins-1/2.

5. Compensation to isotropic shifts and RF errors

5.1. Overview

By examining their respective AH terms, we will inspect the robustness of the various 2Q-recoupling pulse schemes of Fig. 1 to the presence of rf amplitude errors and isotropic shifts. The average Hamiltonians were calculated according to Eq. (41) of the Appendix. The results are summarized in Tables 1–3 for the schemes $R2_2^1$ [19], $R2_4^1$ [20] and CN_n^v used to describe the various 2Q-HORROR implementations of Refs. [18,22], as based on the pulse-elements $\pi, (\pi/2)_0(3\pi/2)_\pi$ and 2π, respectively. Each Table lists the AH terms for isotropic shifts up to third order $\left(\overline{H}_{\mathrm{CS}}^{(n)}; n = 1, 2, 3\right)$ and all cross-terms between rf errors and isotropic shifts to second $\left[\overline{H}_{(\mathrm{CS}\times\mathrm{RF})}^{(2)}\right]$ and third $[\overline{H}_{(\mathrm{CS}\times\mathrm{CS}\times\mathrm{RF})}^{(3)}$ and $\overline{H}_{(\mathrm{CS}\times\mathrm{RF}\times\mathrm{RF})}^{(3)}]$ order, both in the absence and presence of infinitesimally short $\pi/2$ bracketing pulses.

For amplitude-modulated pulse-trains, all AH terms solely involving rf amplitude mis-settings $(H_{\mathrm{RF}}^{\varepsilon})$ vanish identically beyond first order:

$$\overline{H}_{\mathrm{RF}}^{(n)} = 0, n > 1 \quad \text{(amplitude-modulated pulse sequence)} \qquad (24)$$

Furthermore, a cyclic $(U_{\mathrm{RF}}^{\mathrm{nom}}(T, 0) = \mathbf{1})$ amplitude-modulated pulse-sequence associated with zero effective flip angle [e.g., $\beta_\phi\beta_{\phi+\pi}$] fulfill $\overline{H}_{\mathrm{RF}}^{(1)} = 0$ [3]. This holds for all schemes discussed in this paper, except for 2Q-HORRORy [18,22].

Onwards, we use the shorthand form ω_{nut} for the nominal nutation frequency $\omega_{\mathrm{nut,nom}}$. Given the choice of AH analysis in the frame of the rf interaction, $\overline{H}^{(n)}$ is proportional to $\omega_{\mathrm{nut}}^{n-1}$. As ω_{nut} is directly related to the spinning frequency, all expressions in Tables 1–3 may be reformulated as inverse powers of ω_r by making the substitution $\omega_{\mathrm{nut}} \to \omega_r/2$. Depending on the count of the contributing interaction, "CS" or "RF", the nominator of the AH term is proportional to that power of ω_{iso} and ω_ε, respectively. For example, the operator $\overline{H}_{(\mathrm{CS}\times\mathrm{CS}\times\mathrm{RF})}^{(3)} \sim \omega_{\mathrm{iso}}^2\omega_\varepsilon/\omega_{\mathrm{nut}}^2$, whereas $\overline{H}_{(\mathrm{CS}\times\mathrm{RF}\times\mathrm{RF})}^{(3)} \sim \omega_{\mathrm{iso}}\omega_\varepsilon^2/\omega_{\mathrm{nut}}^2$. For the low-power recoupling applications considered here, the AH series expansion (Eq. 36) converges slowly and the high-order terms naturally gain significant influence on the spin dynamics.

5.2. $R2_2^1$ Schemes based on π-pulses

As demonstrated both numerically and experimentally by ^{23}Na and ^{27}Al MAS NMR in Refs. [19,20,29], π-based $R2_2^1$ pulse schemes perform poorly in the simultaneous presence of rf amplitude errors and isotropic shift-differences of a few kHz. Here we show theoretically the underlying reasons for this, focussing initially on the non-bracketed ("plain") pulse sequences as their AH terms convey all relevant information about the 2Q-recoupling performance of the corresponding bracketed schemes [see Eqs. (12) and (13)].

A fundamental problem with the basic $R2_2^1$ pulse sequence is its recoupling of isotropic shifts to first order. It may be verified from Table 1 that phase-inversion supercycling cancels AH terms proportional to transverse spin angular momentum operators S_x and S_y [35,36,40,44], and we showed in Ref. [19] that the shift-recoupling can be eliminated by utilizing $R2_2^1R2_2^{-1}$. Nevertheless, as all higher-order AH terms generated by $R2_2^1$ *also* comprises longitudinal operators (S_z), several cross-terms between rf errors and isotropic shifts remain to second and third order AHT for the $R2_2^1R2_2^{-1}$ supercycle.

Except for the third-order term $\overline{H}_{(\mathrm{CS}\times\mathrm{CS}\times\mathrm{RF})}^{(3)}$, all AH terms of the $R2_2^1R2_2^{-1}$ and $R4_4^2R4_4^{-2}$ pulse schemes are longitudinal, implying that the next stage of "$M = 2$ supercycling" does not cancel them (Table 1). Nevertheless, the numerically simulated 2QF results from $\left(R2_2^1R2_2^{-1}\right)2^1$ and $\left(R4_4^2R4_4^{-2}\right)2^1$ for resonance offset and rf error variations often display significantly improved performance relative to their phase-inversion supercycle-counterparts in the *presence* of quadrupolar interactions. This will be illustrated in the following paper.

A similar peculiar scenario applies for the relationship between the $R2_2^1$ and $R4_4^2$ pulse schemes; the latter is simply a repetition of the former, implying that the two recoupling sequences are associ-

Table 1
Average Hamiltonian terms for supercycled $R2_2^1$ recoupling sequences based on the π_0 inversion element.[a]

	$\overline{H}_{\mathrm{CS}}^{(1)}$	$\overline{H}_{\mathrm{CS}}^{(2)}$	$\overline{H}_{(\mathrm{CS}\times\mathrm{RF})}^{(2)}$	$\overline{H}_{\mathrm{CS}}^{(3)}$	$\overline{H}_{(\mathrm{CS}\times\mathrm{CS}\times\mathrm{RF})}^{(3)}$	$\overline{H}_{(\mathrm{CS}\times\mathrm{RF}\times\mathrm{RF})}^{(3)}$
Pulse sequence						
$R2_2^1 \equiv R4_4^2$	$-\frac{2}{\pi}\omega_{\mathrm{iso}}S_x$	0	$\frac{\omega_{\mathrm{iso}}\omega_\varepsilon}{\omega_{\mathrm{nut}}}\left\{\frac{2}{\pi}S_x - S_z\right\}$	$\frac{\omega_{\mathrm{iso}}^3}{2\omega_{\mathrm{nut}}^2}\left\{\frac{4}{3\pi}S_x - S_z\right\}$	0	$\frac{\omega_{\mathrm{iso}}\omega_\varepsilon^2}{\omega_{\mathrm{nut}}^2}\left\{\frac{(\pi^2-4)}{2\pi}S_x + S_z\right\}$
$R2_2^1R2_2^{-1}$	0	0	$-\frac{\omega_{\mathrm{iso}}\omega_\varepsilon}{\omega_{\mathrm{nut}}}S_z$	$-\frac{\omega_{\mathrm{iso}}^3}{2\omega_{\mathrm{nut}}^2}S_z$	$\frac{2\omega_{\mathrm{iso}}^2\omega_\varepsilon}{\omega_{\mathrm{nut}}^2}S_y$	$\frac{\omega_{\mathrm{iso}}\omega_\varepsilon^2}{\omega_{\mathrm{nut}}^2}S_z$
$R4_4^2R4_4^{-2}$	0	0	$-\frac{\omega_{\mathrm{iso}}\omega_\varepsilon}{\omega_{\mathrm{nut}}}S_z$	$-\frac{\omega_{\mathrm{iso}}^3}{2\omega_{\mathrm{nut}}^2}S_z$	$\frac{4\omega_{\mathrm{iso}}^2\omega_\varepsilon}{\omega_{\mathrm{nut}}^2}S_y$	$\frac{\omega_{\mathrm{iso}}\omega_\varepsilon^2}{\omega_{\mathrm{nut}}^2}S_z$
$(R2_2^1R2_2^{-1})2^1$	0	0	$-\frac{\omega_{\mathrm{iso}}\omega_\varepsilon}{\omega_{\mathrm{nut}}}S_z$	$-\frac{\omega_{\mathrm{iso}}^3}{2\omega_{\mathrm{nut}}^2}S_z$	0	$\frac{\omega_{\mathrm{iso}}\omega_\varepsilon^2}{\omega_{\mathrm{nut}}^2}S_z$
$(R4_4^2R4_4^{-2})2^1$	0	0	$-\frac{\omega_{\mathrm{iso}}\omega_\varepsilon}{\omega_{\mathrm{nut}}}S_z$	$-\frac{\omega_{\mathrm{iso}}^3}{2\omega_{\mathrm{nut}}^2}S_z$	0	$\frac{\omega_{\mathrm{iso}}\omega_\varepsilon^2}{\omega_{\mathrm{nut}}^2}S_z$
Sandwiched[b]						
$R2_2^1 \equiv R4_4^2$	$-\frac{2}{\pi}\omega_{\mathrm{iso}}S_x$	0	$\frac{\omega_{\mathrm{iso}}\omega_\varepsilon}{\omega_{\mathrm{nut}}}\left\{\frac{2}{\pi}S_x + S_y\right\}$	$\frac{\omega_{\mathrm{iso}}^3}{2\omega_{\mathrm{nut}}^2}\left\{\frac{4}{3\pi}S_x + S_y\right\}$	0	$\frac{\omega_{\mathrm{iso}}\omega_\varepsilon^2}{\omega_{\mathrm{nut}}^2}\left\{\frac{(\pi^2-4)}{2\pi}S_x - S_y\right\}$
$R2_2^1R2_2^{-1}$	0	0	$\frac{\omega_{\mathrm{iso}}\omega_\varepsilon}{\omega_{\mathrm{nut}}}S_y$	$\frac{\omega_{\mathrm{iso}}^3}{2\omega_{\mathrm{nut}}^2}S_y$	$\frac{2\omega_{\mathrm{iso}}^2\omega_\varepsilon}{\omega_{\mathrm{nut}}^2}S_z$	$-\frac{\omega_{\mathrm{iso}}\omega_\varepsilon^2}{\omega_{\mathrm{nut}}^2}S_y$
$R4_4^2R4_4^{-2}$	0	0	$\frac{\omega_{\mathrm{iso}}\omega_\varepsilon}{\omega_{\mathrm{nut}}}S_y$	$\frac{\omega_{\mathrm{iso}}^3}{2\omega_{\mathrm{nut}}^2}S_y$	$\frac{4\omega_{\mathrm{iso}}^2\omega_\varepsilon}{\omega_{\mathrm{nut}}^2}S_z$	$-\frac{\omega_{\mathrm{iso}}\omega_\varepsilon^2}{\omega_{\mathrm{nut}}^2}S_y$
$(R2_2^1R2_2^{-1})2^1$	0	0	$\frac{\omega_{\mathrm{iso}}\omega_\varepsilon}{\omega_{\mathrm{nut}}}S_y$	$\frac{\omega_{\mathrm{iso}}^3}{2\omega_{\mathrm{nut}}^2}S_y$	0	$-\frac{\omega_{\mathrm{iso}}\omega_\varepsilon^2}{\omega_{\mathrm{nut}}^2}S_y$
$(R4_4^2R4_4^{-2})2^1$	0	0	$\frac{\omega_{\mathrm{iso}}\omega_\varepsilon}{\omega_{\mathrm{nut}}}S_y$	$\frac{\omega_{\mathrm{iso}}^3}{2\omega_{\mathrm{nut}}^2}S_y$	0	$-\frac{\omega_{\mathrm{iso}}\omega_\varepsilon^2}{\omega_{\mathrm{nut}}^2}S_y$

[a] Isotropic chemical shifts and rf errors are taken into account and (for brevity) given for each sequence as calculated for a single spin-1/2. For a spin-pair, each factor ω_{iso} is for spin j to be replaced by ω_{iso}^j and the operator S_α by $S_{j\alpha}$ $(\alpha = x, y, z)$, and analogously for spin k.
[b] Average Hamiltonian terms for the corresponding pulse sequence $\mathscr{S}$ when bracketed by infinitesimally short $\pi/2$ pulses: $(\pi/2)_\pi\mathscr{S}(\pi/2)_0$.

Table 2
Average Hamiltonian terms for CN_n^ν recoupling sequences based on the cycles specified in column two.[a]

	Cycle	Remark	$\overline{H}_{CS}^{(1)}$	$\overline{H}_{RF}^{(1)}$	$\overline{H}_{CS}^{(2)}$	$\overline{H}_{(CS\times RF)}^{(2)}$	$\overline{H}_{CS}^{(3)}$	$\overline{H}_{(CS\times CS\times RF)}^{(3)}$	$\overline{H}_{(CS\times RF\times RF)}^{(3)}$
Pulse sequence									
$C1_2^0$	$(2\pi)_{\pi/2}$	HORRORy	0	$\omega_\epsilon S_y$	$\frac{\omega_{iso}^2}{2\omega_{nut}}S_y$	$\frac{\omega_{iso}\omega_\epsilon}{\omega_{nut}}S_z$	$\frac{\omega_{iso}^3}{2\omega_{nut}^2}S_z$	$-\frac{\omega_{iso}^2\omega_\epsilon}{\omega_{nut}^2}S_y$	$-\frac{\omega_{iso}\omega_\epsilon^2}{\omega_{nut}^2}S_z$
$C2_{4p}^1$	$(2p\pi)_{\pi/2}$	HORRORy$\bar{y}$[b]	0	0	0	$\frac{\omega_{iso}\omega_\epsilon}{\omega_{nut}}S_z$	$\frac{\omega_{iso}^3}{2\omega_{nut}^2}S_z$	0	$-\frac{\omega_{iso}\omega_\epsilon^2}{\omega_{nut}^2}\{p\pi S_x+S_z\}$
$C2_4^1C2_4^{-1}$	$(2\pi)_{\pi/2}$	HORRORy$\bar{y}\bar{y}$y[c]	0	0	0	$\frac{\omega_{iso}\omega_\epsilon}{\omega_{nut}}S_z$	$\frac{\omega_{iso}^3}{2\omega_{nut}^2}S_z$	0	$-\frac{\omega_{iso}\omega_\epsilon^2}{\omega_{nut}^2}S_z$
Sandwiched[d]									
$C1_2^0$	$(2\pi)_{\pi/2}$	HORRORy	0	$\omega_\epsilon S_z$	$\frac{\omega_{iso}^2}{2\omega_{nut}}S_z$	$-\frac{\omega_{iso}\omega_\epsilon}{\omega_{nut}}S_y$	$-\frac{\omega_{iso}^3}{2\omega_{nut}^2}S_y$	$-\frac{\omega_{iso}^2\omega_\epsilon}{\omega_{nut}^2}S_z$	$\frac{\omega_{iso}\omega_\epsilon^2}{\omega_{nut}^2}S_y$
$C2_{4p}^1$	$(2p\pi)_{\pi/2}$	HORRORy$\bar{y}$	0	0	0	$-\frac{\omega_{iso}\omega_\epsilon}{\omega_{nut}}S_y$	$-\frac{\omega_{iso}^3}{2\omega_{nut}^2}S_y$	0	$\frac{\omega_{iso}\omega_\epsilon^2}{\omega_{nut}^2}\{-p\pi S_x+S_y\}$
$C2_4^1C2_4^{-1}$	$(2\pi)_{\pi/2}$	HORRORy$\bar{y}\bar{y}$y	0	0	0	$-\frac{\omega_{iso}\omega_\epsilon}{\omega_{nut}}S_y$	$-\frac{\omega_{iso}^3}{2\omega_{nut}^2}S_y$	0	$\frac{\omega_{iso}\omega_\epsilon^2}{\omega_{nut}^2}S_y$

[a] See footnote to Table 1 for details on notation. Provided that the 2QC excitation curve is sampled at integer numbers of completed sequences, these pulse trains are representative of 2Q-HORROR and supercycles thereof (column 3).
[b] This implies applying p $(2\pi)_{\pi/2}$ pulses, followed by p $(2\pi)_{3\pi/2}$ pulses; it then corresponds to the HORRORy$\bar{y}$ sequence introduced in Ref. [18], with the option of sampling the 2QF buildup after each completed cycle.
[c] A subsequent stage of supercycling, which may alternatively be interpreted as a $C2_8^1$ sequence based on $C=(2\pi)_{\pi/2}(2\pi)_{3\pi/2}$.
[d] Average Hamiltonian terms for the corresponding pulse sequence when bracketed by infinitesimally short $\pi/2$ pulses: $(\pi/2)_\pi\mathscr{S}(\pi/2)_0$.

Table 3
Average Hamiltonian terms for supercycled $R2_4^1$ recoupling sequences based on the $(\pi/2)_0(3\pi/2)_\pi$ inversion element.[a]

	$\overline{H}_{CS}^{(1)}$	$\overline{H}_{CS}^{(2)}$	$\overline{H}_{(CS\times RF)}^{(2)}$	$\overline{H}_{CS}^{(3)}$	$\overline{H}_{(CS\times CS\times RF)}^{(3)}$	$\overline{H}_{(CS\times RF\times RF)}^{(3)}$
Pulse sequence						
$R2_4^1$	0	0	$-\frac{\omega_{iso}\omega_\epsilon}{\omega_{nut}}S_x$	$-\frac{\omega_{iso}^3}{2\omega_{nut}^2}S_x$	$\frac{\omega_{iso}^2\omega_\epsilon}{\omega_{nut}^2}S_y$	$\frac{\omega_{iso}\omega_\epsilon^2}{\omega_{nut}^2}\{S_x+\frac{\pi}{2}S_z\}$
$R2_4^1R2_4^{-1}$	0	0	0	0	0	$\frac{\pi\omega_{iso}\omega_\epsilon^2}{2\omega_{nut}^2}S_z$
$R2_4^1[\overrightarrow{X},\overleftarrow{X}]$	0	0	0	0	$\frac{\omega_{iso}^2\omega_\epsilon}{\omega_{nut}^2}S_y$	$\frac{\pi\omega_{iso}\omega_\epsilon^2}{2\omega_{nut}^2}S_z$
$(R2_4^1R2_4^{-1})2^1$	0	0	0	0	0	$\frac{\pi\omega_{iso}\omega_\epsilon^2}{2\omega_{nut}^2}S_z$
$(R2_4^1[\overrightarrow{X},\overleftarrow{X}])2^1$	0	0	0	0	0	$\frac{\pi\omega_{iso}\omega_\epsilon^2}{2\omega_{nut}^2}S_z$
Sandwiched[b]						
$R2_4^1$	0	0	$-\frac{\omega_{iso}\omega_\epsilon}{\omega_{nut}}S_x$	$-\frac{\omega_{iso}^3}{2\omega_{nut}^2}S_x$	$\frac{\omega_{iso}^2\omega_\epsilon}{\omega_{nut}^2}S_z$	$\frac{\omega_{iso}\omega_\epsilon^2}{\omega_{nut}^2}\{S_x-\frac{\pi}{2}S_y\}$
$R2_4^1R2_4^{-1}$	0	0	0	0	0	$-\frac{\pi\omega_{iso}\omega_\epsilon^2}{2\omega_{nut}^2}S_y$
$R2_4^1[\overrightarrow{X},\overleftarrow{X}]$	0	0	0	0	$\frac{\omega_{iso}^2\omega_\epsilon}{\omega_{nut}^2}S_z$	$-\frac{\pi\omega_{iso}\omega_\epsilon^2}{2\omega_{nut}^2}S_y$
$(R2_4^1R2_4^{-1})2^1$	0	0	0	0	0	$-\frac{\pi\omega_{iso}\omega_\epsilon^2}{2\omega_{nut}^2}S_y$
$(R2_4^1[\overrightarrow{X},\overleftarrow{X}])2^1$	0	0	0	0	0	$-\frac{\pi\omega_{iso}\omega_\epsilon^2}{2\omega_{nut}^2}S_y$

[a] See footnote to Table 1 for details on notation. The sequences are based on the element $\overrightarrow{X}\equiv(\pi/2)_0(3\pi/2)_\pi$, except for $R2_4^1[\overrightarrow{X},\overleftarrow{X}]$, which is built on a combination of $\overrightarrow{X}$ and $\overleftarrow{X}\equiv(3\pi/2)_0(\pi/2)_\pi$ (see Fig. 1b).
[b] Average Hamiltonian terms for the corresponding pulse sequence $\mathscr{S}$ when bracketed by infinitesimally short $\pi/2$ pulses: $(\pi/2)_\pi\mathscr{S}(\pi/2)_0$.

ated with identical AH terms. Table 1 shows that the same applies for the corresponding phase inversion supercycles, except for the third-order term $\overline{H}_{(CS\times CS\times RF)}^{(3)}$, which is twice as large for $R4_4^2R4_4^{-2}$. Yet, in the presence of quadrupolar interactions, the experimentally observed 2Q-recoupling performance is often better for the $R4_4^2R4_4^{-2}$ pulse train relative to $R2_2^1R2_2^{-1}$, particularly so for spins-5/2 [19,20]. Hence, despite that the present AH analysis makes a dent in understanding many observed relative merits and disadvantages of the 2Q-recoupling options of Refs. [18–20], it fails to explain this feature. Interestingly, Amoureux and co-workers have recently proposed generalized recoupling schemes $RN_N^{N/2}RN_N^{-N/2}$ with $N=2,4,6,\ldots$ (i.e., of which the $R2_2^1R2_2^{-1}$ and $R4_4^2R4_4^{-2}$ schemes of Ref. [19] constitute the first two members) for ^{1}H 2QC excitation [27]. Differences in the resonance-offset compensation between the bracketed and plain schemes were reported, where the latter was concluded to provide superior robustness. The reasons for these observations are unclear, as commented in Section 5.5.

5.3. HORROR supercycles

Table 2 lists the corresponding AH terms for various HORROR recoupling options, each of which may be identified as a 2π-based CN_n^ν sequence. The AH expressions for HORRORy compared with those of HORRORy$\bar{y}$ evidence that the very pronounced 2QF improvements observed experimentally for the latter [18,19,25] stem primarily from the cancellation of the first-order rf error term $\overline{H}_{RF}^{(1)}$ and the second-order shift term $\overline{H}_{CS}^{(2)}$.

Further, experimentally observed ^{23}Na and ^{27}Al 2QF efficiencies from several model samples ($\alpha-Al_2O_3$ and Na_2SO_3 [19]; AlPO-31 [25]) consistently evidenced that when the rf carrier is set such that resonance offsets are small/absent, $R2_2^1R2_2^{-1}$ delivers higher 2QF efficiency than HORRORy$\bar{y}$. However, for increasing resonance offsets, the advantage of $R2_2^1R2_2^{-1}$ over HORRORy$\bar{y}$ shrinks and the effective offset bandwidths of these two recoupling schemes are similar [19,25]. They both perform poorly in cases of even relatively small (a few kHz) differences in resonance frequencies

between the recoupled spins [19,20,25]. As $R2_2^1R2_2^{-1}$ (Table 1) and HORRORy$\bar{y}$ (Table 2) manifest identical error terms to second-order AHT, the primary reason for these observations originate from their differences in $\overline{H}^{(3)}_{(CS\times CS\times RF)}$ and $\overline{H}^{(3)}_{(CS\times RF\times RF)}$. The third-order cross-term $\overline{H}^{(3)}_{(CS\times CS\times RF)}$ vanishes for HORRORy$\bar{y}$, but is significant for $R2_2^1R2_2^{-1}$. On the other hand, the term $\overline{H}^{(3)}_{(CS\times RF\times RF)}$ emphasizes rf error contributions; in the case of the bracketed HORRORy$\bar{y}$ sequence, it comprises an additional term proportional to S_x, that accumulates as τ_{exc} increases. This constitutes the main limiting factor for rf error compensation of HORRORy$\bar{y}$ and leads to much higher susceptibility to rf inhomogeneity compared to the case of $R2_2^1R2_2^{-1}$ applied near resonance. The transverse operator-contribution may be cancelled by another stage of supercycling, denoted by HORRORy$\bar{y}\bar{y}y$ in Table 2 and constituting a $C2_4^1C2_4^{-1}$ sequence based on $C = (2\pi)_{\pi/2}$, or equivalently, $C2_8^1$ symmetry combined with $C = (2\pi)_{\pi/2}(2\pi)_{3/2}$ [Eq. (7)]. We have not evaluated the HORRORy$\bar{y}\bar{y}y$ supercycle further.

For the remaining of this paper and the subsequent one, we focus on the overall superior RN_n^v-based recoupling schemes.

5.4. $R2_4^1$ Schemes based on $(\pi/2)_0(3\pi/2)_\pi$

$R2_4^1$ supercycles based on the inversion element $(\pi/2)_0(3\pi/2)_\pi$ were introduced in Ref. [20] for remedying the susceptibilities of the π-based recoupling schemes. The experimentally (^{23}Na and ^{27}Al NMR) as well as numerically verified improvements achieved by supercycles of $R2_4^1$ stem from their elimination of higher-order AH offset/rf error cross-terms and particularly the leading term $\overline{H}^{(2)}_{(CS\times RF)}$ (Table 3) that plagues both the $R2_2^1R2_2^{-1}$ (Table 1) and HORRORy$\bar{y}$ (Table 2) schemes. We made a misleading statement in Ref. [20], saying that the $\overline{X} = (\pi/2)_0(3\pi/2)_\pi$ composite pulse is "internally compensated for chemical shifts and rf errors". While the element itself is not compensated, it has beneficial properties when combined with $R2_4^1$ symmetry in that both isotropic shifts and rf amplitude errors cancel to first order AHT (Table 3). However, the *basic* $R2_4^1$ scheme possesses the same intrinsic problems of large second-order cross-terms between chemical shifts and rf errors as the $R2_2^1R2_2^{-1}$ sequence.

The reasons for the significant 2Q-recoupling enhancements offered by the $R2_4^1R2_4^{-1}$ and $R2_4^1[\overline{X},\overline{\bar{X}}]$ *supercycles* may be understood as follows: The enhanced robustness to isotropic chemical shifts and rf amplitude errors offered by POST-C7 [52] relative to its parent C7 scheme [50] stems from the observation that the most influential higher-order AH terms of the latter scheme are proportional to longitudinal S_z operators [52]. Consequently, a $\pi/2$-pulse permutation of the original element employed for C7 $[(2\pi)_0(2\pi)_\pi]$ results in $(3\pi/2)_0(2\pi)_\pi(\pi/2)_0$, and in a accompanied rotation of the undesirable longitudinal AH error terms into transverse operators [61,36,52], in analogy with Eq. (12). These terms are subsequently cancelled over the completed C7 cycle [36,52].

A similar scenario applies to the unwanted AH contributions of $R2_2^1R2_2^{-1}$: this pulse sequence is related to $R2_4^1$ by a $\pi/2$-pulse permutation (see Fig. 1). A completed $R2_4^1$ scheme corresponds to a "POST-C" cycle $(\pi/2)_{\pi/2}(2\pi)_{3\pi/2}(3\pi/2)_{\pi/2}$, and its most damaging second- and third-order AH terms involve transverse spin operators (Table 3). They are consequently cancelled over the $R2_4^1R2_4^{-1}$ supercycle, which may alternatively be identified as a "POST-C"-based $C2_8^1$ sequence [Eq. (6)]. In practice, this scheme leads to a dramatically improved compensation to the combined effects of resonance offsets and rf inhomogeneity [20], as will be illustrated further by numerical simulations in Section 6.

Except for $R2_4^1[\overline{X},\overline{\bar{X}}]$, the supercycles based on the composite inversion element $(\pi/2)_0(3\pi/2)_\pi$ annihilate all undesirable AH terms up to third-order AHT but that of $\overline{H}^{(3)}_{(CS\times RF\times RF)}$, which is proportional to S_z for the non-bracketed schemes (Table 3). Hence, this remaining term may be eliminated by a $\pi/2$-pulse permutation, followed by a concatenation of the resulting sequence with its by π phase-shifted counterpart. When applied to the $R2_4^1R2_4^{-1}$ scheme, the result is a $R2_8^1R2_8^{-1}$ sequence based on the composite element $R = (2\pi)_\pi(3\pi/2)_0(\pi/2)_\pi$ and spanning 16 rotational periods. This supercycle cancels all contributions from resonance offsets and rf amplitude errors to third order AHT. As will be discussed elsewhere, the $R2_8^1R2_8^{-1}$ pulse train is promising for "ultra-low-power" broadband 2Q-recoupling of spins-1/2 at very high spinning frequencies. However, in the present context of 2Q-recoupling of half-integer spins, it has hitherto experimentally not offered any improvements relative to the (seemingly inferior) combinations of phase inversion and MQ phase-cycles listed in Table 3. Consequently, we do not consider it in the present work.

5.5. Effects of undesirable linear AH operators

Here we discuss the effects on the 2Q recoupling dynamics from damaging linear angular momentum operators (S_x, S_y, S_z), which stem from the isotropic shifts and their cross-terms with rf errors. The following commutators [35] are relevant:

$$\left[\omega^j_{iso}S_{jz} + \omega^k_{iso}S_{kz}, \left(T^{jk}_{22} + T^{jk}_{2-2}\right)\right] = \left(\omega^j_{iso} + \omega^k_{iso}\right)\left(T^{jk}_{22} - T^{jk}_{2-2}\right) \quad (25)$$

$$\left[\omega^j_{iso}S_{jx} + \omega^k_{iso}S_{kx}, \left(T^{jk}_{22} + T^{jk}_{2-2}\right)\right] = \frac{1}{2}\left\{(\omega^j_{iso} - \omega^k_{iso})\left(-T^{jk}_{11} + T^{jk}_{1-1}\right) + \left(\omega^j_{iso} + \omega^k_{iso}\right)\left(T^{jk}_{21} + T^{jk}_{2-1}\right)\right\} \quad (26)$$

$$\left[\omega^j_{iso}S_{jy} + \omega^k_{iso}S_{ky}, \left(T^{jk}_{22} + T^{jk}_{2-2}\right)\right] = -\frac{i}{2}\left\{\left(\omega^j_{iso} - \omega^k_{iso}\right)\left(T^{jk}_{11} + T^{jk}_{1-1}\right) + \left(\omega^j_{iso} + \omega^k_{iso}\right)\left(T^{jk}_{21} - T^{jk}_{2-1}\right)\right\} \quad (27)$$

where

$$T^{jk}_{1\pm1} = \frac{1}{2}\left(S^{\pm}_j S_{kz} - S_{jz}S^{\pm}_k\right) \quad (28)$$

Accordingly, whenever the AH error term is proportional to $S_{\alpha x}$ or $S_{\alpha y}$ $(\alpha = j, k)$, a non-zero commutator results regardless of the values of ω^j_{iso} and ω^k_{iso}, except in the trivial case of $\omega^j_{iso} = \omega^k_{iso} = 0$. Hence, the presence of AH terms proportional to transverse operators are always detrimental to the 2QC excitation. On the other hand, if the undesirable AH term involves S_z and the carrier frequency is positioned at the mid of the two resonances of spins j and k, $\omega^j_{iso} = -\omega^k_{iso}$ and Eq. (25) vanishes. This property applies to all AH terms comprising *odd* powers of ω^j_{iso} and ω^k_{iso}, and holds for all second and third order terms except for $\overline{H}^{(3)}_{(CS\times CS\times RF)}$. It explains why 2Q dipolar recoupling sequences are prone to tolerating reasonably large differences in isotropic shifts among the recoupled spins, *provided* that the rf carrier is set such that the sum of resonance offsets is (nearly) zero (e.g., see the results of Ref. [52]). Nevertheless, recoupling associated with poor offset-compensation break down rapidly outside of this regime.

As follows from Eq. (12), a non-vanishing AH term of a bracketed pulse sequence is related to that of the basic scheme by a $\pi/2$-rotation around the x-axis. The results of Tables 1–3 mean that a π-based pulse scheme in the absence of bracketing pulses generate AH cross-terms proportional to S_z, which is rotated into transverse components by the bracketing pulses. Therefore, a non-bracketed $R2_2^1$ pulse scheme may in the scenario of small resonance offsets be somewhat better compensated relative to that being sandwiched between $\pi/2$ pulses. However, the differences are expected to be negligible for practical purposes.

Furthermore, in the case of large dipolar interactions in *multi-spin* systems, the non-bracketed recoupling sequences suffer inherent problems from the non-commutation between recoupled ZQ and 2Q terms from *different* spin-pairs. Analogously to Eq. (25), the ZQ terms result in dephasing of the 2QC:

$$\left[T^{jm}_{20}, T^{jk}_{2\pm2}\right] = \pm\frac{1}{\sqrt{6}}\left(T^{jk}_{2\pm2}T^{m}_{10} + T^{j}_{10}T^{km}_{2\pm2}\right) \quad (29)$$

$$= \pm\frac{1}{2\sqrt{6}}\left(S^{\pm}_{j}S^{\pm}_{k}S_{mz} + S_{jz}S^{\pm}_{k}S^{\pm}_{m}\right) \quad (30)$$

For an isolated spin-pair, on the other hand, the commutation of $T^{jk}_{2\pm2}$ and T^{jk}_{20} implies a vanishing influence of the latter on the 2QC dynamics, apart from the factor of 1/2 slower coherence buildup from the non-bracketed pulse sequences [compare Eqs. (21) and (20)]. We have verified both the slower 2QC excitation and the lower 2QF efficiencies delivered by leaving out the bracketing pulses in the contexts of ^{23}Na and ^{27}Al NMR on Na_2SO_3 and $\alpha - Al_2O_3$, respectively (data not shown).

6. Numerical simulations

6.1. Resonance offset variations

Fig. 2 shows numerically calculated CT 2QF responses upon variations in resonance offsets from a pair of $S = 3/2$ subject to increasing differences in isotropic shifts (Δ_{iso}), while applying the *bracketed* pulse sequences (displayed in the right-most panel) for 2QC excitation. All simulations employed the nominal value of the rf nutation frequency $\omega_{nut} = \omega_r/2$: Consequently, as $\omega_\varepsilon = 0$ all differences in the 2QF results among the recoupling sequences stem solely from their respective AH terms $\overline{H}^{(n)}_{CS}$. The results are grouped so as to illustrate the consequence of each supercycling stage (as well as the choice of basic R element); they are examined from the viewpoint of the AH expressions of Tables 1 and 3.

As discussed in the previous section, the compound cycles $R2^1_2$ and $R2^1_4$ are expected to tolerate very small shift-differences: indeed, the 2Q excitation from $R2^1_2$ is perturbed significantly even for $\Delta_{iso} = 2$ kHz (Fig. 2b), whereas the $\overrightarrow{X}$-based scheme $R2^1_4$ offers a slightly enhanced performance (2h) by virtue of its cancellation of resonance offsets to first order AHT (see Table 3). However, no 2QC excitation is observed when Δ_{iso} exceeds ≈2 kHz (Fig. 2i), due to the growing interferences from the third-order term $\overline{H}^{(3)}_{CS}$. For the $R2^1_2R2^{-1}_2$ and $R2^1_4$ schemes, this term only differs in the identity of the respective transverse spin operator. Consequently, these sequences provide essentially identical responses to resonance-offset variations. A rather peculiar behavior is observed for the $R2^1_2$ ($R4^2_4$) scheme in the case of $\Delta_{iso} = 0$ (Fig. 2(a, d)): despite that the 2QF efficiency is perturbed for minute deviations from on-resonance irradiation, decent 2QC signals are obtained for offset-values within a few kHz, even in a regime where the $R2^1_2R2^{-1}_2$ $\left(R4^2_4R4^{-2}_4\right)$ supercycles do not excite 2QC. This feature of $R2^1_2$ probably originates from interferences between the operators $\overline{H}^{(1)}_{CS}$ and $\overline{H}^{(3)}_{CS}$, that carry opposite signs and may partially cancel each other (Table 1).

In the case of the $\overrightarrow{X}$-based sequences, the undesirable term $\overline{H}^{(3)}_{CS}$ is removed by the $R2^1_4R2^{-1}_4$ and $R2^1_4[\overrightarrow{X}, \overleftarrow{X}]$ supercycles, thereby resulting in a significantly enhanced offset compensation (Fig. 2(h, i, k, l)). From Fig. 2(i, l) follows that while the respective effective bandwidths narrow as the isotropic shift-difference grows, the $R2^1_4R2^{-1}_4$ and $R2^1_4[\overrightarrow{X}, \overleftarrow{X}]$ supercycles may excite 2QC within $\Delta_{iso} \lesssim 5$ kHz at the given spinning frequency of 22.5 kHz. In general, 2QC may be generated for shift-differences within $2\pi\Delta_{iso} \lesssim \omega_r/4$, provided that the rf carrier frequency is positioned near the midpoint of the NMR spectrum.

As expected from the AH expressions in Tables 1 and 3, no further improvements of the 2QC excitation are offered by the $M = 2$ supercycles, except in the case of $\left(R2^1_4[\overrightarrow{X}, \overleftarrow{X}]\right)2^1$, which operates

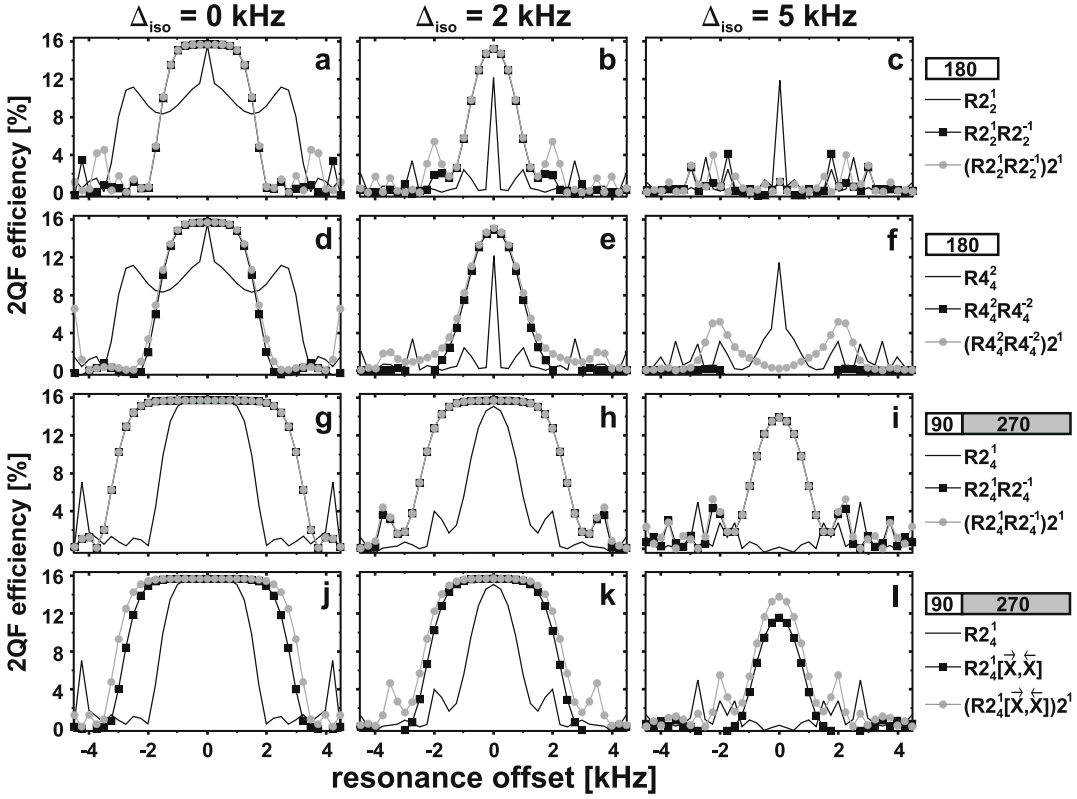

Fig. 2. Numerically simulated 2QF efficiencies for the transfer $S^{CT}_z \rightarrow 2QC^{CT} \rightarrow S^{CT}_z$ versus resonance offset, assuming a powder of $S = 3/2$ spin-pairs subjected to each of the 2Q-recoupling schemes identified in the right-most panel. The calculations were performed for a dipolar coupling constant $b^{jk}/2\pi = -40$ Hz in the absence of quadrupolar interactions at a MAS frequency of 22.5 kHz and using the nominal nutation frequency $\omega^{CT}_{nut}/2\pi = \omega^{RF}_{nut}/2\pi = 11.25$ kHz. Isotropic chemical shift-separations (Δ_{iso}) between the two spins are specified at the top of each panel. 2QF values were sampled around τ_{exc} = 3.5 ms, at the optimum excitation interval for each sequence under the particular condition. The computations were carried out according to Ref. [20], using $\tau^{sel}_{90} = 1.67$ μs and powder averaging was performed over 1154 ZCW orientations [66–68].

equally well as the $R2_4^1R2_4^{-1}$ scheme. While seemingly inferior, a main reason for discussing $R2_4^1[\overrightarrow{X},\overleftarrow{X}]$-based sequences is that experimental ^{27}Al NMR results from both crystalline and amorphous Al-bearing samples indicate that the $R2_4^1[\overrightarrow{X},\overleftarrow{X}]$ scheme often provides higher 2QF signals than $R2_4^1R2_4^{-1}$ [20].

6.2. Rf amplitude errors

Fig. 3 conveys the robustness of each recoupling scheme to rf amplitude mis-settings from its nominal value $\omega_{nut} = \omega_r/2$. In the case of equal chemical shifts of the recoupled spins ($\Delta_{iso} = 0$; left panel of Fig. 3), all sequences perform excellently and admit large deviations ($\pm 20\%$) in the rf amplitudes without significant perturbations of the 2QF amplitudes. The $R2_2^1$ scheme performs overall best, and further supercycling narrows the bandwidth, regardless of whether $R2_2^1$ or $R2_4^1$ compound cycles are considered. The reason is simply that in the absence of other interfering interactions, $R2_2^1$ offers the most rapid alternation between rf phases $\pm\pi/2$ and therefore the fastest compensation mechanism to rf amplitude errors.

However, all $R2_2^1$-based pulse schemes perform very poorly even for minute chemical shift-differences, and an erratic 2QC excitation results (Fig. 3; middle panel). It originates from the second-order cross-term between isotropic shifts and rf errors (Table 1). As for the susceptibility with respect to resonance offsets in Fig. 2, the basic $R2_4^1$ scheme also gives poor 2QC excitation due to this cross-term. However, as discussed above, this term is together with most damaging third-order AH terms cancelled by phase-inversion supercycling, and a significantly better performance of the $R2_4^1R2_4^{-1}$ pulse scheme is observed. Yet, in the presence of larger shift differences (Fig. 3(i, l)), the rf error compensation is only reasonably good. As observed for the offset-compensation, the MQ phase-cycle $\left(R2_4^1[\overrightarrow{X},\overleftarrow{X}]\right)2^1$ offers some improvements relative to $R2_4^1[\overrightarrow{X},\overleftarrow{X}]$, particularly for the case of $\Delta_{iso} = 5$ kHz (Fig. 3l). This by due to cancellation of the $\overline{H}^{(3)}_{(CS\times CS\times RF)}$ term of the latter scheme.

7. Conclusions

We have presented average Hamiltonian expressions that explain several differences observed in the experimental 2QF responses to rf inhomogeneity and resonance offsets for the HORROR$y\bar{y}$ [18], $R2_2^1R2_2^{-1}$ [19], $R2_4^1R2_4^{-1}$ and $R2_4^1[\overrightarrow{X},\overleftarrow{X}]$ [20] supercycles, as previously evaluated numerically and experimentally in Refs. [19,20,25]. Our analytical results were also supported by numerically exact computer simulations of the 2QF efficiency on variations of rf errors and resonance offsets, which further confirmed the superiority of the $R2_4^1$-based supercycles of Ref. [20]. Their favorable features compared to the HORROR$y\bar{y}$ and $R2_2^1R2_2^{-1}$ pulse sequences originate from better suppression of high-order AH cross-terms between isotropic shifts and rf amplitude errors.

Nevertheless, as simplified AHT calculations may have limited predictability for applications to half-integer quadrupolar spins in rigid solids, the AHT results of this study will be complemented by numerical simulations and ^{23}Na and ^{27}Al MAS NMR experiments in the following paper: we will then directly explore the consequences of first and second-order quadrupolar interactions

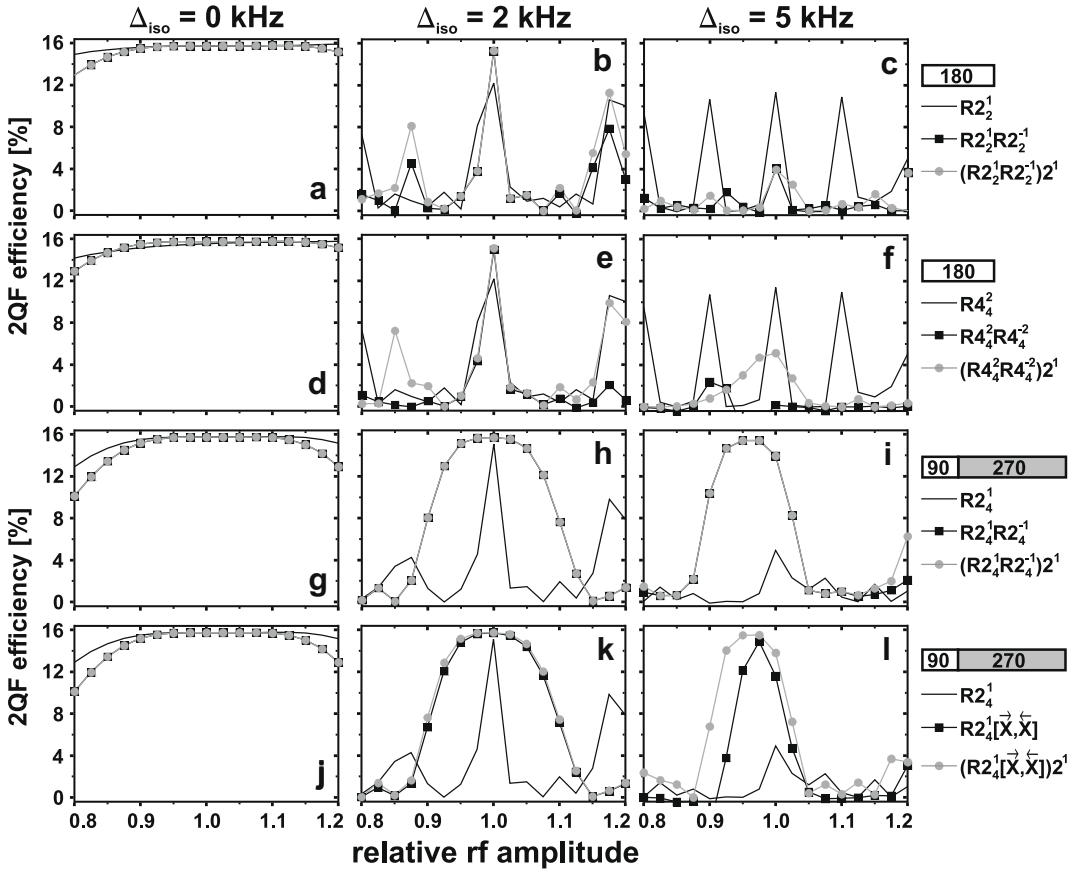

Fig. 3. Simulations using identical parameters as in Fig. 2, but instead varying the ratio $\omega_{nut}/\omega_{nut,nom}$ between the rf nutation frequency relative to its nominal value of $\omega_{nut,nom} = \omega_r/2$. The rf carrier was for each sequence positioned at its optimal resonance offset (see Fig. 2); for $\Delta_{iso} \neq 0$ this generally corresponded to the midpoint of the two resonances.

on the dipolar recoupling as well as its dependence on the external magnetic field.

Further, some results presented here give guidance to the promises and limitations of utilizing (very) low rf-power supercycles operating at the HORROR-condition ($\omega_{\rm nut}^{\rm RF} = \omega_r/2$) for driving homonuclear recoupling among dilute spins-1/2 at the ultra-fast MAS frequencies (>60 kHz) currently available. Low-power recoupling is particularly important for applications to biological systems where concerns about the sample integrity is crucial due to the heating from rf fields applied on *at least one* [62], and usually two, rf channels: for the latter case, the rf-demands for recoupling the dilute spins demands a factor of three higher ^{1}H nutation frequencies for removal of interfering heteronuclear couplings [51,63,64].

Acknowledgments

This work was supported by the Swedish Research Council (VR) and the Carl Trygger Foundation. A.Y.H. Lo was supported by a postdoctoral grant from the Wenner-Gren Foundations.

Appendix A

Here the basic calculations underlying the AH terms presented in Sections 4 and 5 are outlined. They follow the same treatments as reviewed in numerous publications (e.g., see [32–34]), but add some features to facilitate evaluations of high-order AH terms in spin systems involving several interactions. AHT is also specifically developed for RN_n^ν and CN_n^ν classes of symmetry-based pulse sequences [3,37], including their supercycles discussed in this work [40,41,45]. However, the present AH description does not follow that usually employed in the context of symmetry-based recoupling; rather, the simplicity of the present pulse sequences (low N) in conjunction with a sole consideration of spatially time-independent interactions (isotropic chemical shifts and rf errors) readily allows for a "traditional" AH description up to third order in the Magnus expansion [65].

A.1. Interaction-frame Hamiltonian

Employing the notation of Section 3.1, the rotating-frame spin Hamiltonian may be expressed

$$H(t) = \sum_j^{N_{\rm int}} H_{\Lambda_j}(t) + H_{\rm RF}^{\rm nom}(t) + H_{\rm RF}^{\varepsilon}(t) \tag{31}$$

where $N_{\rm int}$ is the number of distinct spin interactions Λ in a multi-spin system. Following the well-established framework of AHT [32,33], we first transform the spin Hamiltonian into an interaction-frame defined by the "ideal" rf contribution, $H_{\rm RF}^{\rm nom}(t)$, by applying

$$\widetilde{H}(t) = U_{\rm RF}^{\rm nom}(t,0)^{-1} H(t) U_{\rm RF}^{\rm nom}(t,0) + i\left\{\frac{d}{dt} U_{\rm RF}^{\rm nom}(t,0)^{-1}\right\} U_{\rm RF}^{\rm nom}(t,0) \tag{32}$$

with the rf pulse propagator given by

$$U_{\rm RF}^{\rm nom}(t,0) = \widehat{T}\exp\left\{-i\int_0^t dt' H_{\rm RF}^{\rm nom}(t')\right\}. \tag{33}$$

and $\widehat{T}$ representing the Dyson time-ordering (super)operator. The last term in Eq. (32) cancels $H_{\rm RF}^{\rm nom}(t)$ of the rotating-frame Hamiltonian, meaning that each of the individual Hamiltonians $\widetilde{H}_\Lambda(t)$ may be obtained directly by the following operator sandwich:

$$\widetilde{H}_\Lambda(t) = U_{\rm RF}^{\rm nom}(t,0)^{-1} H_\Lambda(t) U_{\rm RF}^{\rm nom}(t,0). \tag{34}$$

During the pth pulse (Section 3.1), the interaction-frame rf error Hamiltonian is given by

$$\widetilde{H}_{\rm RF}^{\varepsilon} = H_{\rm RF}^{\varepsilon} = \omega_\varepsilon R_z(\phi_p) S_x R_z(-\phi_p), \quad t_{p-1} \leqslant t < t_p. \tag{35}$$

A.2. Average Hamiltonian expansion

The time-independent AH of the interaction-frame Hamiltonian [Eq. (32)] is derived from the Magnus expansion [65]

$$\overline{\widetilde{H}} = \overline{\widetilde{H}}^{(1)} + \overline{\widetilde{H}}^{(2)} + \overline{\widetilde{H}}^{(3)} + \ldots \tag{36}$$

The nth order AH term comprises nested commutators between the various interaction-frame Hamiltonians $\widetilde{H}_{\Lambda_j}(t), \widetilde{H}_{\Lambda_k}(t), \ldots$ of the spin system, including the rf error terms. The first-order AH of interaction Λ corresponds to its time-average over the pulse sequence [32,33]

$$\overline{\widetilde{H}}_\Lambda^{(1)} = \frac{1}{T}\int_0^T dt \widetilde{H}_\Lambda(t) \tag{37}$$

whereas the second-order AH contribution is a sum over all cross-terms involving two interactions Λ_j and Λ_k:

$$\overline{\widetilde{H}}_{\Lambda_j\times\Lambda_k}^{(2)} = -\frac{i}{2T}\int_0^T dt \int_0^t dt' \left[\widetilde{H}_{\Lambda_j}(t), \widetilde{H}_{\Lambda_k}(t')\right] \tag{38}$$

The *order* of interactions is important in Eq. (38), as $\overline{\widetilde{H}}_{\Lambda_j\times\Lambda_k}^{(2)}$ and $\overline{\widetilde{H}}_{\Lambda_k\times\Lambda_j}^{(2)}$ are not necessarily equal and generally both terms need to be evaluated. An exception applies to "auto-correlation" terms, i.e., when $\Lambda_j = \Lambda_k$. They are for brevity denoted $\overline{\widetilde{H}}_{\Lambda_j}^{(n)}$. The third-order AH involve sums over ordered triplets of interactions, $\Lambda_j \times \Lambda_k \times \Lambda_m$, for which either *none*, *two* (e.g., $\Lambda_j \times \Lambda_k \times \Lambda_j$), or *all* of the interactions may be equal. Such a triplet is given by [32,33]

$$\overline{\widetilde{H}}_{\Lambda_j\times\Lambda_k\times\Lambda_m}^{(3)} = -\frac{1}{6T}\int_0^T dt \int_0^t dt' \int_0^{t'} dt'' \left[\widetilde{H}_{\Lambda_j}(t), \left[\widetilde{H}_{\Lambda_k}(t'), \widetilde{H}_{\Lambda_m}(t'')\right]\right] + \left[\left[\widetilde{H}_{\Lambda_j}(t), \widetilde{H}_{\Lambda_k}(t')\right], \widetilde{H}_{\Lambda_m}(t'')\right] \tag{39}$$

While formally Eq. (36) appears concise, it generally comprises a sum over a large number of terms, where the summation is to be taken over all combinations of interactions, including permutations of their orders:

$$\overline{\widetilde{H}} = \sum_{\Lambda_j,\Lambda_k,\Lambda_m,\ldots} \overline{\widetilde{H}}_{\Lambda_j}^{(1)} + \overline{\widetilde{H}}_{\Lambda_j\times\Lambda_k}^{(2)} + \overline{\widetilde{H}}_{\Lambda_k\times\Lambda_j}^{(2)} + \overline{\widetilde{H}}_{\Lambda_j\times\Lambda_j\times\Lambda_m}^{(3)} + \overline{\widetilde{H}}_{\Lambda_j\times\Lambda_k\times\Lambda_m}^{(3)} + \ldots \tag{40}$$

The number of terms contributing to $\overline{\widetilde{H}}_{\Lambda_j\times\Lambda_k\times\ldots}^{(n)}$ grows rapidly with n and the number $N_{\rm int}$ of spin interactions considered.

A.3. Symmetrized average Hamiltonian terms

For a convenient book-keeping of the various terms contributing to each AH order, we define a "symmetrized" [40] nth-order AH term involving q distinct interactions according to

$$\overline{\widetilde{H}}^{(n)}\underbrace{(\Lambda_j \times \Lambda_k \times \Lambda_m \times \ldots)}_{q \text{ distinct } \Lambda} = \sum_{\substack{\text{all permutations}\\ \text{of interactions}}} \overline{\widetilde{H}}_{\Lambda_j\times\Lambda_k\times\Lambda_m\times\ldots}^{(n)} \tag{41}$$

Each Hamiltonian term involves forming an n-tuple of interactions, where q interactions out of the total number $N_{\rm int}$ are selected, with the restriction that $q \leqslant n$. Next, the sum is carried out over *all* permutations of *ordered* cross-terms, which ensures that all AH terms between the q interactions are considered for the given perturbation order. Once the symmetrized AH terms are formed, the order of interactions specified within the parenthesis is unimportant, as

for instance, $\overline{\widetilde{H}}^{(n)}_{(\Lambda_j\times\Lambda_k\times\Lambda_m\times\ldots)} = \overline{\widetilde{H}}^{(n)}_{(\Lambda_m\times\Lambda_j\times\Lambda_k\times\ldots)}$. For example, for two distinct interactions Λ_j and Λ_k, the symmetrized second-order AH term is [40]

$$\overline{\widetilde{H}}^{(2)}_{(\Lambda_j\times\Lambda_k)} = \overline{\widetilde{H}}^{(2)}_{\Lambda_j\times\Lambda_k} + \overline{\widetilde{H}}^{(2)}_{\Lambda_k\times\Lambda_j}. \tag{42}$$

A symmetrized third-order AH cross-term between *three* distinct interactions is a sum over 3!=6 "ordered" terms,

$$\begin{aligned}\overline{\widetilde{H}}^{(3)}_{(\Lambda_j\times\Lambda_k\times\Lambda_m)} = {} & \overline{\widetilde{H}}^{(3)}_{\Lambda_j\times\Lambda_k\times\Lambda_m} + \overline{\widetilde{H}}^{(3)}_{\Lambda_j\times\Lambda_m\times\Lambda_k} + \overline{\widetilde{H}}^{(3)}_{\Lambda_k\times\Lambda_j\times\Lambda_m} + \overline{\widetilde{H}}^{(3)}_{\Lambda_k\times\Lambda_m\times\Lambda_j} \\ & + \overline{\widetilde{H}}^{(3)}_{\Lambda_m\times\Lambda_j\times\Lambda_k} + \overline{\widetilde{H}}^{(3)}_{\Lambda_m\times\Lambda_k\times\Lambda_j}\end{aligned} \tag{43}$$

whereas that involving only *two* interactions (Λ_j and Λ_k) results from three ordered terms:

$$\overline{\widetilde{H}}^{(3)}_{(\Lambda_j\times\Lambda_j\times\Lambda_k)} = \overline{\widetilde{H}}^{(3)}_{\Lambda_j\times\Lambda_j\times\Lambda_k} + \overline{\widetilde{H}}^{(3)}_{\Lambda_j\times\Lambda_k\times\Lambda_j} + \overline{\widetilde{H}}^{(3)}_{\Lambda_k\times\Lambda_j\times\Lambda_j}. \tag{44}$$

Note that $\overline{\widetilde{H}}^{(3)}_{(\Lambda_j\times\Lambda_j\times\Lambda_k)}$, for which Λ_j appears twice, is distinct from $\overline{\widetilde{H}}^{(3)}_{(\Lambda_j\times\Lambda_k\times\Lambda_k)}$ (Λ_k appearing twice). If "auto-correlation" terms are considered, we employ the shorthand notation $\overline{\widetilde{H}}^{(3)}_{\Lambda_j} \equiv \overline{\widetilde{H}}^{(3)}_{\Lambda_j\times\Lambda_j\times\Lambda_j} = \overline{\widetilde{H}}^{(3)}_{(\Lambda_j\times\Lambda_j\times\Lambda_j)}$; then for each AH order n, the symmetrized AH is identical to the corresponding "ordered" AH term.

This symmetrized AH formulation presents an advantage of clearly separating the various contributions to a particular AH order and provides a convenient recipe for generating a given term representing the interference between any specific combination of spin interactions. The AH expressions found in most of the literature (e.g., see [33–36]) implies inserting Eq. (32)—i.e., the sum over all interaction-frame Hamiltonians—into Eqs. (37)–(39). The commutator expressions in Eqs. (38) and (39) then directly results in all AH terms up to third order in Eq. (40). While simpler notation-wise and in principle straightforward to calculate, the analytical evaluations often becomes impractically complex. For example, considering cross-terms between isotropic chemical shifts (CS) and rf amplitude errors (RF), there are two distinct third-order contributions: $\overline{H}^{(3)}_{(\mathrm{CS}\times\mathrm{CS}\times\mathrm{RF})}$ and $\overline{H}^{(3)}_{(\mathrm{CS}\times\mathrm{RF}\times\mathrm{RF})}$. Eq. (44) provides a straightforward route to forming each of these based on Eq. (39). On the other hand, if Eqs. (31), (32) and (39) are combined and evaluated for a sum of chemical shift and rf error Hamiltonians, the net result is equivalent to separately forming four symmetrized third-order AH terms: $\overline{H}^{(3)}_{\mathrm{CS}}$, $\overline{H}^{(3)}_{\mathrm{RF}}$, $\overline{H}^{(3)}_{(\mathrm{CS}\times\mathrm{CS}\times\mathrm{RF})}$ and $\overline{H}^{(3)}_{(\mathrm{CS}\times\mathrm{RF}\times\mathrm{RF})}$, of which the latter two originate from three ordered AH terms [see Eq. (44)]. So notation aside, there is nothing fundamentally new with the present formulation of the AH terms.

Refs. [33–37,61] reviews various relationships between a given rf pulse sequence and the transformation properties of the corresponding interaction-frame Hamiltonian and their implications for the resulting AH.

Appendix B. Supplementary data

Supplementary data associated with this article can be found, in the online version, at doi:10.1016/j.jmr.2009.07.007.

References

[1] A.E. Bennett, R.G. Griffin, S. Vega, Recoupling of homo- and heteronuclear dipolar interactions in rotating solids, NMR Basic Princ. Prog. 33 (1994) 1–77.
[2] S. Dusold, A. Sebald, Dipolar recoupling under magic-angle-spinning conditions, Ann. Rep. NMR Spectrosc. 41 (2000) 185–264.
[3] M.H. Levitt, Symmetry-based pulse sequences in magic-angle spinning solid state NMR, Encyclopedia of NMR. Vol 9: Advances in NMR (2002) 165–196.
[4] M.J. Duer, Determination of structural data from multiple-quantum magic-angle-spinning NMR experiments, Chem. Phys. Lett. 277 (1997) 167–174.
[5] M. Nijman, M. Ernst, A.P.M. Kentgens, B.H. Meier, Rotational-resonance NMR experiments in half-integer quadrupolar spin systems, Mol. Phys. 98 (2000) 161–178.
[6] Z. Gan, P. Robyr, Deuterium polarization transfer in rotating solids and its application in structural investigation, Mol. Phys. 95 (1998) 1143–1152.
[7] G. Facey, D. Gusev, R.H. Morris, S. Macholl, G. Buntkowsky, ^{2}H MAS NMR of strongly dipolar coupled deuterium pairs in transition metal dihydrides: extracting dipolar coupling and quadrupolar tensor orientations from the lineshape of spinning sidebands, Phys. Chem. Chem. Phys. 2 (2000) 935–941.
[8] N.G. Dowell, S.E. Ashbrook, J. McManus, S. Wimperis, Relative orientation of quadrupole tensors from two-dimensional multiple-quantum MAS NMR, J. Am. Chem. Soc. 123 (2001) 8135–8136.
[9] M. Edén, L. Frydman, Quadrupolar-driven recoupling of homonuclear dipolar interactions in the nuclear magnetic resonance of rotating solids, J. Chem. Phys. 114 (2001) 4116–4123.
[10] M. Edén, J. Grinshtein, L. Frydman, High resolution 3D exchange NMR spectroscopy and the mapping of connectivities between half-integer quadrupolar nuclei, J. Am. Chem. Soc. 124 (2002) 9708–9709.
[11] H.-T. Kwak, P. Srinivasan, J. Quine, D. Massiot, Z. Gan, Satellite transition rotational resonance of homonuclear quadrupolar spins: magic-angle effect on spin-echo decay and inversion recovery, Chem. Phys. Lett. 376 (2003) 75–82.
[12] M. Edén, L. Frydman, Homonuclear NMR correlations between half-integer quadrupolar nuclei undergoing magic-angle spinning, J. Phys. Chem. B 107 (2003) 14598–14611.
[13] S.E. Ashbrook, M.J. Duer, Structural information from quadrupolar nuclei in solid state NMR, Concepts Magn. Reson. A 28 (2006) 183–248.
[14] M. Edén, H. Annersten, Å. Zazzi, Pulse-assisted homonuclear dipolar recoupling of half-integer quadrupolar spins in magic-angle spinning NMR, Chem. Phys. Lett. 410 (2005) 24–30.
[15] M. Baldus, D. Rovnyak, R.G. Griffin, Radio-frequency-mediated dipolar recoupling among half-integer quadrupolar spins, J. Chem. Phys. 112 (2000) 5902–5909.
[16] S. Wi, J.W. Logan, D. Sakellariou, J.D. Walls, A. Pines, Rotary resonance recoupling for half-integer quadrupolar nuclei in solid-state nuclear magnetic resonance, J. Chem. Phys. 117 (2002) 7024–7033.
[17] A.J. Painter, M.J. Duer, Double-quantum-filtered nuclear magnetic resonance spectroscopy applied to quadrupolar nuclei in solids, J. Chem. Phys. 116 (2002) 710–722.
[18] G. Mali, G. Fink, F. Taulelle, Double-quantum homonuclear correlation magic angle sample spinning nuclear magnetic resonance spectroscopy of dipolar-coupled quadrupolar nuclei, J. Chem. Phys. 120 (2004) 2835–2845.
[19] M. Edén, D. Zhou, J. Yu, Improved double-quantum NMR correlation spectroscopy of dipolar-coupled quadrupolar spins, Chem. Phys. Lett. 431 (2006) 397–403.
[20] A.Y.H. Lo, M. Edén, Efficient symmetry-based homonuclear dipolar recoupling of quadrupolar spins: Double-quantum NMR correlations in amorphous solids, Phys. Chem. Chem. Phys. 10 (2008) 6635–6644.
[21] M. Edén, Homonuclear dipolar recoupling of half-integer spin quadrupolar nuclei: techniques and applications, Solid State NMR (2009), doi:10.1016/j.ssnmr.2009.06.005.
[22] N.C. Nielsen, H. Bildsoe, H.J. Jakobsen, M.H. Levitt, Double-quantum homonuclear rotary resonance: efficient dipolar recovery in magic-angle-spinning nuclear magnetic resonance, J. Chem. Phys. 101 (1994) 1805.
[23] K. Takegoshi, K. Nomura, T. Terao, Rotational resonance in the tilted rotating frame, Chem. Phys. Lett. 232 (1995) 424–428.
[24] K. Takegoshi, K. Nomura, T. Terao, Selctive homonuclear polarization transfer in the tilted rotating frame under magic angle spinning in solids, J. Magn. Reson. 127 (1997) 206–216.
[25] G. Mali, V. Kaucic, F. Taulelle, Measuring distances between half-integer quadrupolar nuclei and detecting relative orientations of quadrupolar and dipolar tensors by double-quantum homonuclear recoupling nuclear magnetic resonance experiments, J. Chem. Phys. 128 (2008) 204503.
[26] M. Edén, Determination of absolute quadrupolar tensor orientations by double-quantum NMR on powders, Chem. Phys. Lett. 470 (2009) 318–324.
[27] B. Hu, Q. Wang, O. Lafon, J. Trébosc, F. Deng, J.-P. Amoureux, Robust and efficient spin-locked symmetry-based double-quantum homonuclear dipolar recoupling for probing ^{1}H–^{1}H proximities in the solid-state, J. Magn. Reson. 198 (2009) 41–48.
[28] A. Samoson, E. Lippmaa, A. Pines, High resolution solid-state NMR. Averaging of second-order effects by means of a double rotor, Mol. Phys. 65 (1988) 1013–1018.
[29] A. Brinkmann, A.P.M. Kentgens, T. Anupold, A. Samoson, Symmetry-based recoupling in double rotation solid-state NMR spectroscopy, J. Chem. Phys. 129 (2008) 174507.
[30] A.J. Vega, MAS NMR spin locking of half-integer quadrupolar nuclei, J. Magn. Reson. 96 (1992) 50–68.
[31] J.D. Walls, K.H. Lim, A. Pines, Theoretical studies of the spin dynamics of quadrupolar nuclei at rotational resonance conditions, J. Chem. Phys. 116 (2002) 79–90.
[32] U. Haeberlen, J.S. Waugh, Coherent averaging effects in magnetic resonance, Phys. Rev. 175 (1968) 453–467.
[33] U. Haeberlen, High Resolution NMR in Solids. Selective Averaging, Academic Press, New York, 1976.
[34] D.P. Burum, W.K. Rhim, Analysis of multiple pulse NMR in solids III, J. Chem. Phys. 71 (1979) 944–956.

[35] M. Hohwy, N.C. Nielsen, Elimination of high order terms in multiple pulse nuclear magnetic resonance spectroscopy: application to homonuclear decoupling in solids, J. Chem. Phys. 106 (1997) 7571.
[36] M. Hohwy, N.C. Nielsen, Systematic design and evaluation of multiple-pulse experiments in nuclear magnetic resonance spectroscopy using a semi-continuous Baker–Campbell–Hausdorff expansion, J. Chem. Phys. 109 (1998) 3780–3791.
[37] M.H. Levitt, Symmetry in the design of NMR multiple-pulse sequences, J. Chem. Phys. 128 (2008) 052205.
[38] M. Edén, M.H. Levitt, Pulse sequence symmetries in the nuclear magnetic resonance of spinning solids: application to heteronuclear decoupling, J. Chem. Phys. 111 (1999) 1511–1519.
[39] M. Carravetta, M. Edén, X. Zhao, A. Brinkmann, M.H. Levitt, Symmetry principles for the design of radiofrequency pulse sequences in the nuclear magnetic resonance of rotating solids, Chem. Phys. Lett. 321 (2000) 205–215.
[40] A. Brinkmann, M. Edén, Second order average Hamiltonian theory of symmetry-based pulse schemes in the nuclear magnetic resonance of rotating solids: application to triple-quantum dipolar recoupling, J. Chem. Phys. 120 (2004) 11726–11744.
[41] P.E. Kristiansen, M. Carravetta, J.D. van Beek, W.C. Lai, M.H. Levitt, Theory and applications of supercycled symmetry-based recoupling sequences in solid-state nuclear magnetic resonance, J. Chem. Phys. 124 (2006) 234510.
[42] A. Brinkmann, J. Schmedt auf der Günne, M.H. Levitt, Homonuclear zero-quantum recoupling in fast magic-angle-spinning nuclear magnetic resonance, J. Magn. Reson. 156 (2002) 79–96.
[43] W.S. Warren, D.P. Weitekamp, A. Pines, Theory of selective excitation of multiple-quantum transitions, J. Chem. Phys. 73 (1980) 2084–2099.
[44] M. Carravetta, M. Edén, O.G. Johannessen, H. Luthman, P.J.E. Verdegem, J. Lugtenburg, A. Sebald, M.H. Levitt, Estimation of carbon–carbon bond lengths and medium-range internuclear distances by solid-state nuclear magnetic resonance, J. Am. Chem. Soc. 123 (2001) 10628–10638.
[45] M. Edén, Order-selective multiple-quantum excitation in magic-angle spinning NMR: creating triple-quantum coherences with a trilinear Hamiltonian, Chem. Phys. Lett. 366 (2002) 469–476.
[46] M. Edén, A. Brinkmann, Triple-quantum dynamics in multiple-spin systems undergoing magic-angle spinning: application to ^{13}C homonuclear correlation spectroscopy, J. Magn. Reson. 173 (2005) 259–279.
[47] D.A. Varshalovich, A.N. Moskalev, V.K. Khersonskii, Quantum Theory of Angular Momentum, World Scientific, Singapore, 1988.
[48] M. Edén, Computer simulations in solid state NMR: I. Spin dynamics theory, Concepts Magn. Reson. A 17 (2003) 117–154.
[49] J. Lin, M.J. Bayro, R.G. Griffin, N. Khaneja, Dipolar recoupling in solid-state NMR by phase alternating pulse sequences, J. Magn. Reson. 197 (2009) 145–152.
[50] Y.K. Lee, N.D. Kurur, M. Helmle, O.G. Johannessen, N.C. Nielsen, M.H. Levitt, Efficient dipolar recoupling in the NMR of rotating solids. A sevenfold symmetric radiofrequency pulse sequence, Chem. Phys. Lett. 242 (1995) 304–309.
[51] C.M. Rienstra, M.E. Hatcher, L.J. Mueller, B. Sun, S.W. Fesik, R.G. Griffin, Efficient multispin homonuclear double-quantum recoupling for magic-angle-spinning NMR: ^{13}C–^{13}C correlation spectroscopy of U–^{13}C-eryhromycin, J. Am. Chem. Soc. 120 (1998) 10602–10612.
[52] M. Hohwy, H.J. Jakobsen, M. Edén, M.H. Levitt, N.C. Nielsen, Broadband dipolar recoupling in the nuclear magnetic resonance of rotating solids: a compensated C7 pulse sequence, J. Chem. Phys. 108 (1998) 2686–2694.
[53] M. Hohwy, C.M. Rienstra, C.P. Jaroniec, R.G. Griffin, Fivefold symmetric homonuclear dipolar recoupling in rotating solids: application to double quantum spectroscopy, J. Chem. Phys. 110 (1999) 7983–7992.
[54] A. Brinkmann, M. Edén, M.H. Levitt, Synchronous helical pulse sequences in magic-angle-spinning NMR. Double quantum spectroscopy of recoupled multiple-spin systems, J. Chem. Phys. 112 (2000) 8539–8554.
[55] M. Edén, Enhanced symmetry-based dipolar recoupling in solid-state NMR, Chem. Phys. Lett. 378 (2003) 55–64.
[56] P.E. Kristiansen, M. Carravetta, W.C. Lai, M.H. Levitt, A robust pulse sequence for the determination of small homonuclear dipolar couplings in magic-angle spinning NMR, Chem. Phys. Lett. 390 (2004) 1–7.
[57] P.E. Kristiansen, D.J. Mitchell, J.N.S. Evans, Double-quantum dipolar recoupling at high magic-angle spinning rates, J. Magn. Reson. 157 (2002) 253–266.
[58] D.M. Gregory, D.J. Mitchell, J.A. Stringer, S. Kiihne, J.C. Shiels, J. Callahan, M.A. Metha, G.P. Drobny, Windowless dipolar recoupling: the detection of weak dipolar couplings between spin 1/2 nuclei with large chemical shift anisotropies, Chem. Phys. Lett. 246 (1995) 654–663.
[59] B.-Q. Sun, P.R. Costa, D. Kocisko, P.T. Lansbury, R.G. Griffin, Internuclear distance measurements in solid state nuclear magnetic resonance: dipolar recoupling via rotor synchronized spin locking, J. Chem. Phys. 102 (1995) 702–707.
[60] M. Feike, D.E. Demco, R. Graf, J. Gottwald, S. Hafner, H.W. Spiess, Broadband multiple-quantum NMR spectroscopy, J. Magn. Reson. A 122 (1996) 214–221.
[61] M.H. Levitt, R. Freeman, T. Frenkiel, Broadband decoupling in high-resolution nuclear magnetic resonance spectroscopy, Adv. Magn. Reson. 11 (1983) 47–110.
[62] C.E. Hughes, S. Luca, M. Baldus, Radio-frequency driven polarization transfer without heteronuclear decoupling in rotating solids, Chem. Phys. Lett. 385 (2004) 435–440.
[63] Y. Ishii, J. Ashida, T. Terao, ^{13}C–^{1}H dipolar recoupling dynamics in ^{13}C multiple-pulse solid-state NMR, Chem. Phys. Lett. 246 (1995) 439–445.
[64] A.E. Bennett, C.M. Rienstra, J.M. Griffiths, W. Zen, P.T. Lansbury Jr., R.G. Griffin, Homonuclear radio frequency-driven recoupling in rotating solids, J. Chem. Phys. 108 (1998) 9463–9479.
[65] W. Magnus, On the exponential solution of differential equations for a linear operator, Com. Pure. Appl. Math. 7 (1954) 649–673.
[66] S.K. Zaremba, Good lattice points, discrepancy, and numerical integration, Ann. Mat. Pura. Appl. 73 (4) (1966) 293–317.
[67] H. Conroy, Molecular Schrödinger equation. VIII. A new method for the evaluation of multidimensional integrals, J. Chem. Phys. 47 (1967) 5307–5318.
[68] V.B. Cheng, H.H. Suzukawa, M. Wolfsberg, Investigations of a nonrandom numerical method for multidimensional integration, J. Chem. Phys. 59 (1973) 3992–3999.